Scottish Universities Environmental Research Centre

STATISTICAL AND IMAGING METHODS FOR LUMINESCENCE DETECTION OF IRRADIATED INGREDIENTS.
Reference No CSA 5240

D.C.W. Sanderson, L.A. Carmichael, S.D. Murphy, V.H. Whitley, E.M. Scott, A.J. Cresswell

Final Report

East Kilbride Glasgow G75 OQF Telephone: 01355 223332 Fax: 01355 229898

Contents

Summary

This project investigated two potential approaches to improving the reliability of luminescence methods for detecting minor irradiated ingredients in foods. Whereas in the 1980's there were no validated methods for laboratory detection of irradiated foods, work conducted in the UK and elsewhere by the mid 1990's had resulted in the development of a series of physical, chemical and biological methods capable of detecting a range of irradiated food classes. Of these the luminescence methods embodied in EN1788 (Thermoluminescence) and EN13751 (Photostimulated luminescence) standards have been applied to detection of a variety of products including herbs and spices, and seafood. In common with the other EN standard methods almost all validation work had been originally conducted using pure irradiated or unirradiated ingredients. Yet application experience had shown the presence of mixed products containing both irradiated and unirradiated ingredients. A short study was commissioned by MAFF to investigate the impact of blending on standard EN1788 methods, and on the provisional draft EN13751 (the standard having been published in the meantime) method. This showed the impact of dilution of irradiated material between 10% and 0.1% concentrations on detection rates, which unsurprisingly are reduced by extreme dilution. UK labelling regulation, both before and after adoption of the European Directive on Food Irradiation, call for labelling of all irradiated ingredients regardless of concentration or origin within the final product. This study was therefore motivated by the recognition of the long term need for improved methods to improve reliability at low concentrations.

Two complementary approaches were investigated. The project first examined whether TL data collected using the EN1788 method could be enhanced using advanced statistical procedures. Data sets from the SURRC TL archive, and from project CSA4790 were used both to define the characteristics of irradiated and unirradiated end members, and to assess classification methods using the controlled blending experimental data sets of CSA 4790. Multivariate analyses, based on principal components analysis and discriminant analysis of glow curve data; kinetic deconvolution approaches coupled to PCA and DA, and neural analyses were investigated and compared with detection rates achieved using expert visual classification. To complement this experiments were undertaken to explore the potential of using focussed laser stimulation to produce spatially resolved measurements from mineral grains separated from foods. Two systems were evaluated based on IR and visible band lasers. Work was undertaken to explore sample presentation and to assess the ability of this approach to distinguish mixtures of irradiated and unirradiated grains.

The statistical work was successful in developing three approaches which could be used for objective identification of irradiated materials. Pure irradiated and unirradiated data sets from 150 sample pairs were obtained having searched the SUERC archive of more than 3500 luminescence analyses. These were used to set up multivariate analyses based on the approaches outlined above. Performance in recognising irradiated ingredients using these methods was then assessed with data drawn from the MAFF blending investigation, comprising 160 permutations of irradiated and unirradiated herbs and spices at 10%, 1% and 0.1% concentrations. It was possible to achieve good detection rates with all statistical approaches, the best approaches investigated being the use of glow curve deconvolution coupled with linear discrimination, and the use of neural approaches. The absolute performance achieved matched that of expert visual classification utilising the revised EN1788 criteria, which were adopted within the international standard during the course of this project. The use of advanced statistical methods, while not adding performance, can provide objective support to visual classifications. During performance assessment it was also noted that the performance

of all methods was sufficiently close to infer that detections rates are most dependent on the statistical presence or absence of irradiated grains within the extracted samples used for TL analysis. This raises practical suggestions for improving detection rates at low concentrations based on the use of larger samples and more specific mineral separation approaches. These may be worth investigating further.

Laser scanning approaches were also investigated using highly focussed laser beams to stimulated luminescence sequentially from different parts of separated mineral samples. Work was conducted using a system which had been developed in earlier work at SUERC, and then followed by additional investigation using an improved instrument built during the project. Initial work confirmed the feasibility of using laser scanning approaches to obtain spatially resolved luminescence data at or near the dimensions of individual mineral grains. Practical obstacles included the recognition that laser scattering from surfaces coated with mineral grains introduced an element of cross-talk between different parts of the sample, and difficulties in accurate re-positioning of the sample using the first generation prototype instrument. Work was conducted to investigate a series of different sample presentation media to improve the former, and to incorporate high precision mechanical and optoelectronic means of re-positioning samples between initial measurements, external irradiation, and subsequent re-measurement. Both IR and visible band semiconductor lasers were investigated with successful production of single grain images. The short and medium term reliability of the lasers used was acceptable. The lasers used both however eventually failed, which suggests that long term lifetime may be an issue for further work. Of the two lasers the IR laser in particular gave a good signal to background ratio for discriminating between irradiated and unirradiated grains. Quantitative analysis of the grain resolved images confirms the potential of this approach in identifying minor irradiated components.

The overall conclusions of the work are that both statistical approaches and imaging instruments are able to enhance current methods. The observation that visual classification can match the performance even of deconvolution or neural approaches suggests that future effort should be directed more towards improvement of grain statistics in conventional measurements, and in further development and investigation of imaging approaches. In these ways it can anticipated that the performance of standard luminescence methods for detecting dilute mixtures of irradiated and unirradiated food ingredients could be significantly improved. To do so would further enhance work conducted by FSA and other bodies to ensure that regulations governing the use of irradiation in food processing and the labelling of imported foods are followed.

List of Figures

List of Tables

1. Introduction

This report summarises work performed under Project CSA 5240 aimed at developing new and improved techniques to detect blended mixtures of herbs spices and seasonings containing irradiated products.

Herbs, spices and seasonings are commonly treated with ionising radiation to provide an effective means of reducing undesirable microbiological loads without reducing organoleptic properties. Herbs and spices are products with diverse sources and a multinational supply and distribution chain. They are frequently mixed either to consolidate batches or to produce consistent colour, quality of flavours or used in seasonings and compound foods. For all these reasons irradiated herbs and spices can find their way into dilute mixtures in the food chain, presenting a different range of analytical problems from those associated with pure irradiated products.

UK and European legislation[1,2] call for unambiguous declaration of irradiated products and ingredients both at each stage in the supply chain and at point of sale. Presently, validated methods[3,4] for detecting irradiated foods have been specifically developed for pure irradiated products and do not address the problem of blending. Blended products, especially those which have a minor irradiated component within an unirradiated matrix, could dramatically affect whether the sample would be identified as irradiated or not, using standard criteria.

The aim of the project is to address the difficulties presented by bulk or polymineral silicate samples, using statistical approaches to TL and PSL analyses. Single grain imaging methods will also be investigated, as this offers a way of distinguishing between individual irradiated and unirradiated components from compound food samples.

Current validated TL methods use a combination of first glow shape and glow ratio to identify blends. The main identification criteria being the presence of TL first glow component associated with unstable charge carriers. An approach to try and improve the objectivity is the use of statistical analysis on glow shape. Three methods of glow shape analysis have been identified; multivariate techniques, kinetic deconvolution, and neural networks; which should, in principle, improve the detection rate for minor blends and result in a more objective set of classification criteria.

These methods will initially be evaluated using data sets from well-characterised unirradiated and irradiated samples of many product types and origins, providing a basis for assessing each method. The introduction of a series of blended materials prepared under CSA4790[5], representing combinations of sensitivity and concentration of both unirradiated and irradiated material will provide a means of evaluating the performance of each of the statistical methods.

Blended mixtures will have a mixed population of irradiated and unirradiated grains of different sizes and mineral species. In recognition of these factors, it is expected that single grain analysis by both TL and PSL methods would provide a discrete set of data for both the irradiated and unirradiated components within the sample. The approach presently being taken is to stimulate luminescence sequentially from individual grains using IR stimulation and a motorised XY micrometer stage. Initial work has been ongoing, development and optimisation of data presentation and collection, using standard irradiated and unirradiated F1

feldspar. Further work includes the presentation of blended F1 at 0.1%, 1%, 10% and 50% concentrations.

Section 2 of this report gives details of the statistical approaches used and how well they perform. Section 3 describes the exploratory PSL imaging approach showing scans obtained from unirradiated and irradiated material. The work has been conducted in several stages. Initial work with a first generation laboratory system capable of IR stimulation and imaging confirmed the general concept for production of images. However sample presentation with respect to laser scattering effects was identified as an issues requiring attention. A number of approaches to deal with this have been explored, leading to the development of a system utilising small pits drilled in a carrier plate. A second generation imaging instrument has been developed, which is capable of multiple samples measurements, and also of configuration with near IR, VIS and CO-2 lasers for PSL imaging and potentially single grain TL measurements. This system has so far been evaluated with a green laser source, which together with the IR work confirms the general validity of the imaging concept. In section 4 conclusions are drawn about the statistical approaches, and the status of PSL imaging system as a potential tool for further development.

2. Statistical Approaches

2.1 Outline of approaches

The first part of this project looked at using statistical methods to identify the presence of irradiated components using data collected from existing machines using standard methods. Three initial approaches were suggested in an attempt to increase the correct classification of the recent irradiation history of submitted food samples as compared to current techniques. These three approaches are:

- Multivariate Analysis
- Deconvolution (Inverse Problem solutions)
- Neural Analysis.

2.2 Data Sets

The study has been designed with the objective of trying to improve the detection criteria on samples, prepared using standard TL and PSL methods[3,4], which contain an irradiated component. The aim is examine statistical approaches using glow shapes. For this study two standard data sets needed to be selected; one as a training set, which will contain unirradiated and irradiated samples to establish initial statistical parameters. The second set will contain samples with known concentrations of irradiated material for performance testing.

For over a decade, research into TL and PSL detection methods for irradiated food has been ongoing at SURRC. Data sets and retained samples for over 3500 samples have been systematically recorded and more recently transferred to an ACCESS database. The database contains details of each sample submitted from external organizations for irradiation testing, samples purchased for PSL research and instrument kits, samples purchased for interlaboratory trials and samples purchased for MAFF funded research – which include several hundred UK purchased samples prior to the time food irradiation was permitted.

These samples are prepared implementing the standard EN13751 PSL and EN 1788 and V27 TL methods, and their data sets represent authentic unirradiated, irradiated and blended samples. All samples have a unique laboratory code, which can be cross-correlated to their measured TL and PSL data and classification. The TL data is recorded for both first and second (normalised to 1kGy) from room temperature to 400°C at a heating rate of 5°C/s; with the net glow curve (the background automatically being subtracted from the sample glow curve) stored. The sample is identified using EN1788 criteria, which depends on the glow ratio (G1/G2) and the shape of the first glow (G1). The temperature interval for evaluation of the TL glow ratio is in the range of 150°C to 250°C.

A selection of TL data was identified from the database, which would use as the basis for the training set. The initial set contained 150 data (75 duplicate analyses) for both unirradiated and irradiated herbs and spices containing first, second glow curves and glow ratio for the complete glow curve. For the initial set we were trying to obtain an evenly balanced number of pure herbs and spices; containing 8 herb products of parsley, sage, oregano, rosemary, thyme, mixed herbs, chives and basil, and ten spice products of cinnamon, black pepper, white pepper, paprika, ginger, turmeric, cayenne, garlic, nutmeg, onion, chilli and cumin.

The data for the training set was extracted and reintegrated into 10°C bands between 0 and 400°C temperature range for statistical analysis; thus each glow curve can be represented by a vector of 40 elements. The training set was then closely examined to ensure that we had well characterised and a representative data set; with several data being rejected due to having major electrical spikes, low sensitivity and outliers. The data for the training set was then plotted to ensure that there was unambiguous separation between the unirradiated and irradiated samples (Figure 2.1) and this set would be used in the exploratory statistical analyses to evaluate performance.

An evaluation data set is required to test how well the statistical methods perform in comparison with standard methods. An ideal set would be the retained blended samples and data collected from project CSA4790. Samples of six products (oregano, basil, sage, paprika, ginger and cinnamon) were prepared combining irradiated material at three different concentrations – 10%, 1% and 0.1% with unirradiated material under controlled conditions and the data recorded for both TL and PSL. The PSL analyses followed the EU standard method, and the TL analyses were conducted relative to the EN1788 and MAFF V27 protocols. Results presented in CSA4790[5] show that standard methods are able to detect a significant proportion of irradiated blends at concentrations above 1-10%, however below these concentrations there is a significant probability of non-detection, particularly for low sensitivity components.

Again, data for the evaluation set used net curves for the temperature region 0-400°C, which were then reintegrated into 10°C temperature bands for the statistical analysis.

Both the training and evaluation data sets provide a starting point for exploring statistical approaches to data analysis and for evaluating performance.

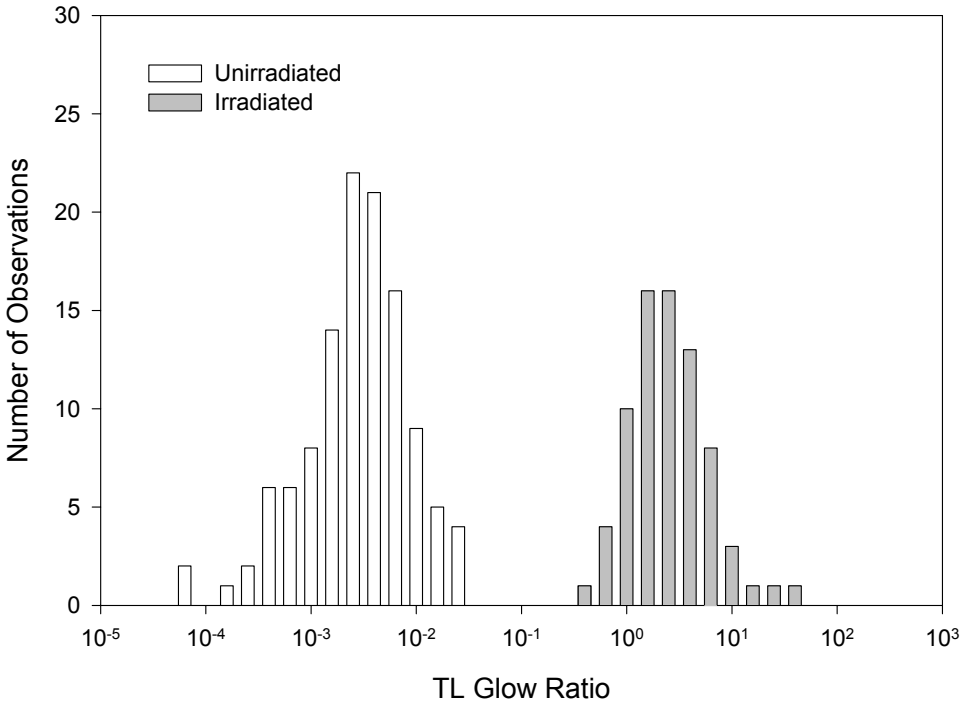

Figure 2.1: Glow ratio histogram for training set containing 110 unirradiated and 82 irradiated analyses

2.3 Multivariate Analysis

Principle components analysis can be used to examine the relationships among a set of *p* correlated variables. Transforming the original set of variables does this; in this application the 40 temperature values or the 40 deconvolved energy values, into a new set of uncorrelated variables called principal components. These new variables are linear combinations of the original variables and are generally listed in order of amount of variance that each components accounts. This transformation is in fact an orthogonal rotation in *p*-space.

The objective is to see if the first few components account for most of the variation in the original data. If they do, then the effective dimensionality of the data is less than *p*. This situation arises when the original variables are highly correlated. In this application, there will be a rather large correlation among the variables. This correlation arises because each TL peak in the data set will extend over all temperature values. For example, the variables at 390 °C and 400 °C say the same thing because they both measure the same TL from peaks occurring at other temperature values.

To do the analysis, the principle components of the 'irradiated' and 'unirradiated' data were first found. Figure 2.2 shows a plot of the first three principle components determined from the deconvolved data. The first principle component can be described as the difference between low energy and high energy populated traps. The second principal component can be roughly described as the negative first derivative of the deconvolved data.

The first three principle components are an orthogonal rotation of the data in three-dimensional space.

Figure 2.3 shows the result of this rotation formed from the first three principle components of the deconvolved data. Two clusters of data are seen in the figure, one cluster of the irradiated data and one cluster of the unirradiated data. This illustrates that the dimensionality of the problem can be reduced from a large number of beginning variables down to a few further analysis. Together, these seven components accounted for 99% of the variation in the data.

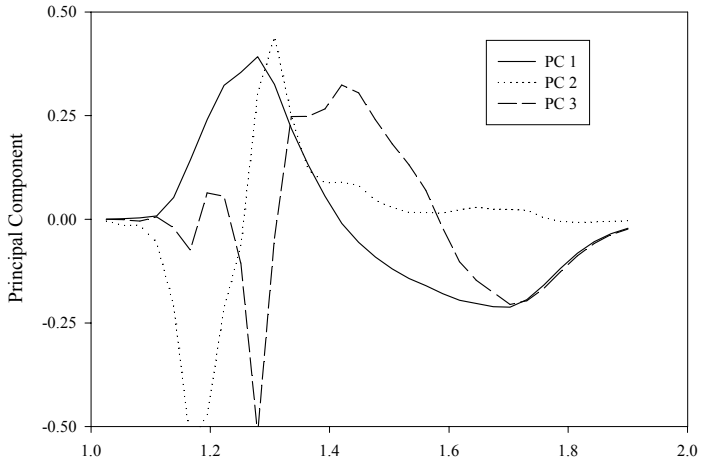

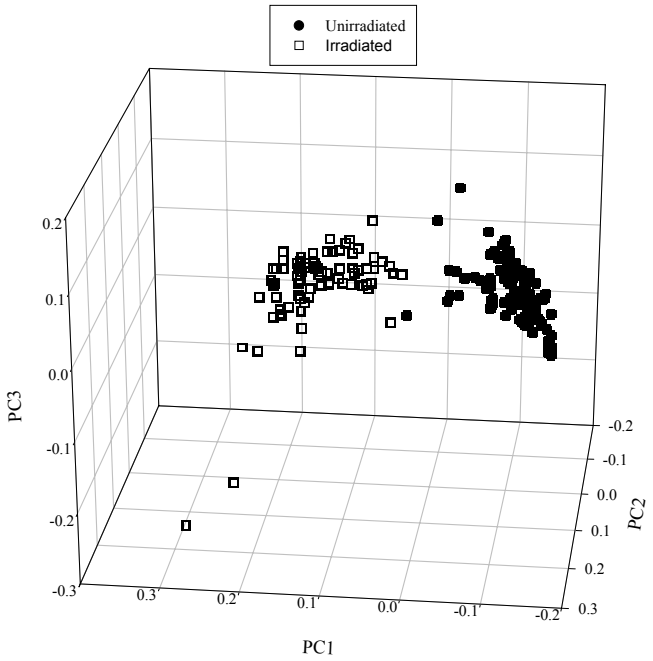

Figure 2.3: First three principal components of the deconvolved training set data

The first three principle components accounted for roughly 94% of the variation in the data. In order to ensure that some of the outliers were not misclassified, a total of seven principle components were used for further analysis.

Once these seven principle components were determined, they were then used with Discriminate Analysis to classify the 10 %, 1 % and 0.1 % mixtures.

2.4 Deconvolution approaches

In deconvolution, a series of Randall-Wilkins[6,7] peaks are used to model the data. The major difficulty with this approach is correctly determining the number of peaks to accurately fit the data. However, by introducing an activation energy and attempt-to-escape frequency distribution of the captured carrier population g[E,s], the number of peaks does not need to be known.

Based on the assumption that the intensity of TL is described by a superposition of Randall-Wilkins functions RW[E,s], the relationship between the charge carrier population g[E,s] and the TL intensity I[T,β] is:

$$I[T,\beta] = \iint g[E,s]RW[E,s,T,\beta]dEds \qquad (1)$$

where the Randall-Wilkins function is given by:

$$RW[E,s,T,\beta] = n_0 s Exp[-\frac{E}{kT}]\frac{s}{\beta} Exp\left[-\frac{E}{kT} - \int_{To}^{T} Exp[-\frac{E}{k\theta}]d\theta\right]. \qquad (2)$$

Here n_0 is the initial trapped charge concentration at time t=0, β is the heating rate, E is the thermal depth of the populated trap, s is the attempt-to-escape frequency, T is the temperature, k is Boltzmann's constant, and θ is a dummy integration variable.

Eq.(1) belongs to a class of Fredholm[8] integral equations of the first kind. The equation may also be regarded as an integral transformation between the spaces of (E,s) and the measurable (T, β), which in operator notation is written as:

$$Kg[E,s] = I[T,\beta] \qquad (3)$$

where the linear operator K is defined in eq.(1).

Eq.(3) is then solved by using a non-negative least squares procedure (NNLS)[9], where the additional constraint of the non-negativity of the amplitudes g[E,s] is taken into account.

Unfortunately, the TL is only weakly dependent upon the heating rate. In order to correctly solve eq.(3), there should be several orders of magnitude difference between the highest and lowest heating rates used. Because of physical constraints upon the equipment, the highest heating rates that can be used do not exceed about 10 K/s. Thus, one must use slow heating rates in order to achieve the necessary separation in the heating rates. This leads to a dramatic increase in the amount of time necessary to process a single sample (from a few minutes to the order of weeks).

Because of this problem, a fixed value for the frequency factor has been used. By fixing the frequency factor, the populated trap distribution can be obtained from a single TL data set. Unfortunately, this means that if the frequency factor used is incorrect, then the determined energy depths will not be correct either. While this would be a problem in many other applications, it does not prove to be a problem here. The exact thermal depths or frequency factors of the populated traps do not need to be determined. It is only necessary to know if there is charge in the thermally unstable† traps. If there is charge in thermally unstable traps, it will show up in the deconvolution indicating that the material was recently irradiated.

Figure 2.4 shows an example of the conversion of experimental data in temperature space converted to energy space. The TL peak was created using four traps at 0.95, 1.0, 1.05, and 1.1 eV respectively and an initial population of $n_0 = 1.0$ in each trap. In temperature space, the traps combine to produce one broad, indistinct TL peak. It would be difficult to correctly determine the number of contributing states in temperature space. In energy space, however, each trap is distinctly seen making it much easier to determine the number of components contributing to the TL. For a more in-depth discussion of the use of these techniques, see the work of Larson *et al*.[10]

† Thermally unstable here refers to traps that are shallow enough that all trapped charge will leak out over a short time span (e.g. one year)

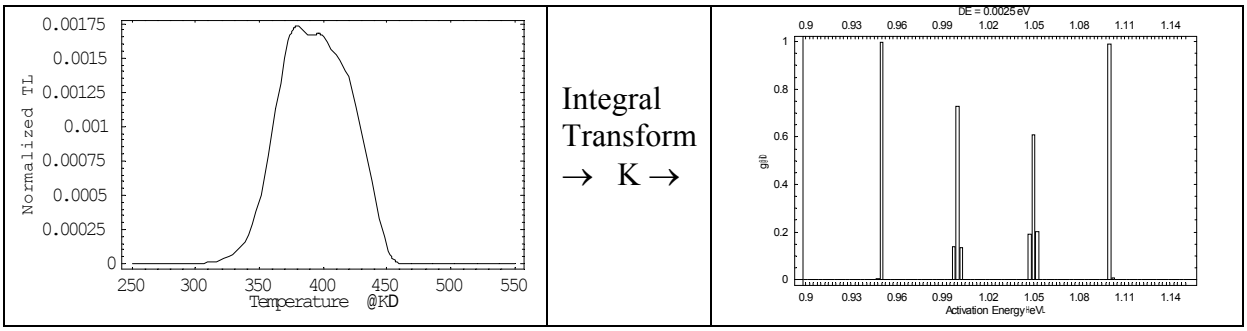

Figure 2.4: Illustration of the conversion from temperature space to energy space.

Figure 2.5a shows a deconvolution of a sample that is classified as 'unirradiated'. The energy range used for the deconvolution was 40 bins over the range of 0.9 eV-1.8 eV and a frequency factor of $s = 10^{11}$. The bulk of the trapped charge is found distributed around 1.6 eV. There is a small tail extending to the shallower energy region, but there is little trapped charge below the range of 1.3 eV. Figure 2.5b shows the measured TL used to perform the deconvolution.

Figure 2.6a shows the deconvolution for a material that is classified as 'irradiated'. The parameters used to deconvolve the TL were identical to the ones used for the 'unirradiated' material. Again, there seems to be a distribution of trapped charges around 1.6 eV. However, there is a much higher concentration of charge localized in the shallower traps in the range of 1.1eV – 1.36eV. This region corresponds to a depth that is thermally unstable. The presence of charge in these traps strongly indicates the presence of an irradiation event within the past year.

2.5 Neural Analysis

Another approach identified at the outset was the potential of applying neural network approaches to classification of data sets from blended products. While the underlying principles and procedures involved are different from those of conventional multivariate approaches, neural systems can be used for adaptive classification criteria based on training sets and for pattern recognition. A potential advantage of these approaches compared with standard multivariate methods is their ability to exploit non-linear relationships within the data sets, which are expected to be a characterisation of luminescence systems.

This section outlines exploratory work to implement and evaluate a neural approach to the problem. In principle the neural systems can be applied to new data, reduced data in the form of integrated data, normalised data, or deconvoluted data.

Neural Analysis can be broadly described as a technique that tries to relate the shape of the TL data with the group status (irradiated or unirradiated). The field of study is very broad and the number of possible networks that one can use is quite large.

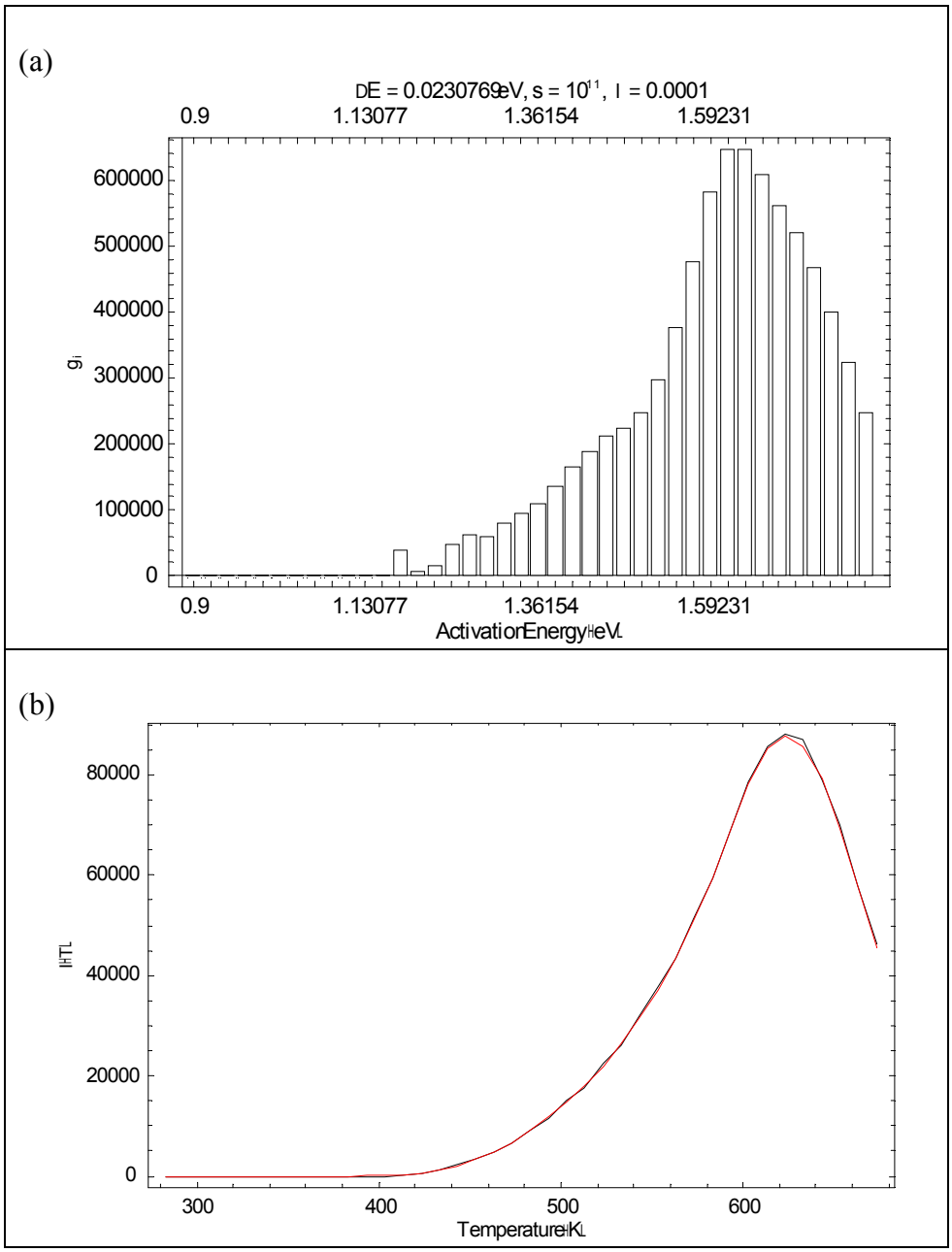

Figure 2.5: Deconvolution of an 'unirradiated' material. Here, (a) shows the deconvolution and (b) shows the experimentally measured TL used for the deconvolution

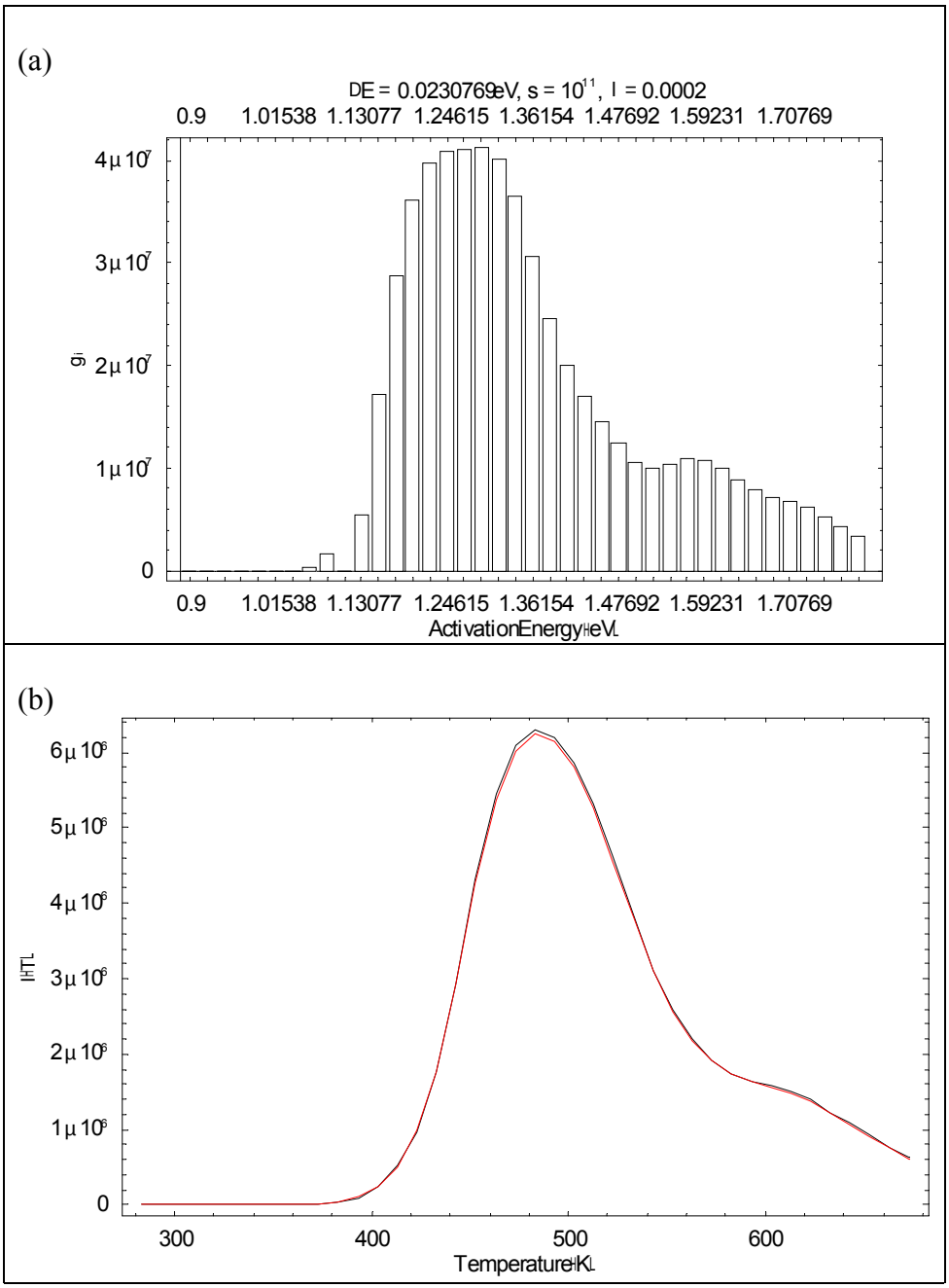

Figure 2.6: Deconvolution of an 'irradiated' material. Here, (a) shows the deconvolution and (b) shows the experimentally measured TL used for the deconvolution

The most difficult part of the task is determining the correct network to use. The most promising of the networks found for this application were Back Propagation Network (BPN), Probability Neural Networks (PNN), and Adaptive Resonance Theory (ART). This is not an exhaustive list of neural networks that could be used for classification of food irradiation. Because of time constraints only a few methods were considered and only one method was tested – BPN. BPN was tested first because it is the most widely used of the various algorithms, ensuring that 3rd party software employing the BPN algorithm will not be difficult to find. This, however, does not mean that BPN is necessarily the best neural network to use for these applications.

A schematic of the Back Propagation Network is shown in Figure 2.7. The circles represent nodes (neurons) that perform an identical action on all of its inputs. The arrows represent weighted data being moved from one node to another.

The network is trained by presenting the training pattern (in this case, a complete set of irradiated and unirradiated data vectors) to the input layer of the network. Initially, random weighting values are chosen and the information is propagated forward through the network to determine the actual network outputs determined by the random weights.

The error terms are calculated on the output layers and the gradient of the error surface with respect to each of the output-layer weights is found. Next, the gradient of the error surface with respect to each of the weights on the hidden layers is calculated. This is where the concept of back propagation formally enters. The errors on the output layer are calculated first, then those errors are brought back to the hidden layer to calculate the surface gradient there.

Once the gradients have been calculated, each weight value is adjusted a small amount in the direction of the negative of the gradient. Then, the next input pattern is presented and the weight-update process is repeated. This is carried on until all the output-layer errors have been reduced to an acceptable value, at which point the neural network has determined opti-

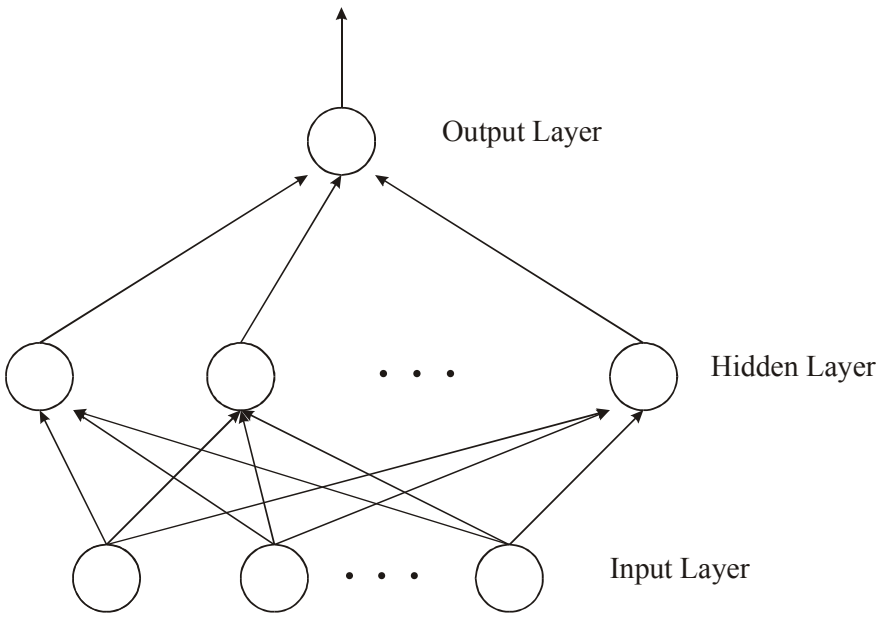

Figure 2.7: Schematic diagram of a Back Propagation Network

mal weights. For a more technical introduction, a large number of books are available that cover BPN, such as the one by Bishop[11].

In this application, custom code was written and used to evaluate the effectiveness of the back propagation algorithm in correctly predicting the irradiation state of the material. The number of input nodes (neurons) used was the 40 different TL intensities taken over the heating range of 10-400 °C or the 32 inputs if only the temperature ranges of 90-400°C were used. The number of nodes in the hidden layer is variable and chosen such that it minimized the errors in classification the greatest. More than one hidden layer can be used and could increase the accuracy of determination. However, additional layers were not tested because of the additional computation time involved in weight determination and as the performance of the back propagation using only a single hidden layer was already very good. Because of the way the algorithm works, input data must be between 0 and 1. Thus, only normalized data could be tested.

A series of 190 training vectors (110 irradiated, 80 unirradiated) along with their correct irradiation states was used to train the network. Figure 2.8 illustrates the value of the output errors during the training of the network. It is seen that the algorithm is able to adapt the weights such there is a considerable minimization of errors in correctly classifying the two irradiation states.

2.5.1 Data constraining

A considerable amount of time was spent trying to determine the cause of outliers and to help control these problem points and misidentifications associated with them.

Initially, all of the training data set was checked and any sets that were questionable were removed. Of the remaining sets, all of the TL curves were checked for spurious glitches and corrected if any were found. In the end, 110 fully unirradiated, 82 fully irradiated, 105 10%-irradiated mixtures, 100 1%-irradiated mixtures, and 98 0.1%-irradiated mixtures remained.

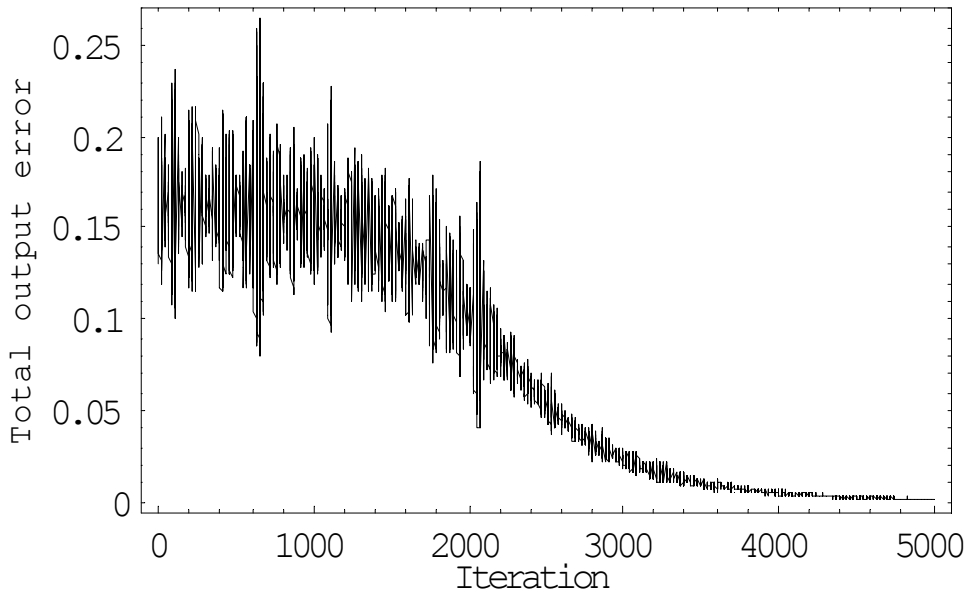

Figure 2.8: Calculated output errors after each iteration through the BPN network

When normalizing the data to unit area, it is necessary to ensure that there is indeed an irradiated signal present. If a TL signal that consists of only background noise is normalized to unit area, one is then making noise comparable to a true TL signal. This will lead to outliers where there should be none. In order to overcome this problem, 3x the background counts (assumed to be 50 counts.s^{-1}) were subtracted off the data sets and any bins with a negative count were set to zero. This ensured that noise in the measurements did not have a large effect when normalised, yet the amount was small enough that it did not unduly bias the data. This is justified because most of the TL maximums were in the range of 10^3-10^7 counts.s^{-1}, thus 10^2 is at least an order of magnitude smaller than the low end of the TL range.

When calculating ratios, it was necessary to smooth the data before hand. Because the unsmoothed ratios are not properly constrained, each TL curve is not merely a measure of the luminescence emitted by the sample, but the luminescence emitted by the sample plus random noise α. The *i*th component of the TL glow ratio r_i can be approximated by:

$$r_i = \frac{TL_1[i]+\alpha_1[i]}{TL_2[i]+\alpha_2[i]} \approx \begin{cases} \dfrac{TL_1[i]}{TL_2[i]} & TL_1[i] >> \alpha_1[i],\ TL_2[i] >> \alpha_2[i] \\ \dfrac{\alpha_1[i]}{\alpha_2[i]} & \alpha_1[i] >> TL_1[i],\ \alpha_2[i] >> TL_2[i] \end{cases} \tag{4}$$

In areas of the glow curve where there is no TL, the glow ratio is a ratio of the noise in the data. In the experimental data, there is little luminescence below the temperature range of ~90°C but there was a large number of large glow ratios in this region because of the unconstrained nature of the data. In order to overcome this problem, the temperature values below 90°C were not used, and the remaining data were smoothed to ensure that noise did not distort the glow ratios.

It is imperative that the glow curves do not become distorted during the smoothing. Several different smoothing methods were tried in order to determine the method that best smoothed the data without introducing distortions. The methods tried were moving averages, Bezier spline interpolation, moving Bezier spline interpolation, Fourier filtering, and finally deconvolution smoothing.

Moving averages worked very well as long as long as the 2nd derivative of the data was approximately zero. However, in places where the 2nd derivative was quite large (e.g. at the wings of the TL curves and at the peak), moving averages introduced a large amount of distortion in the data.

Three types of Bezier spline interpolation were tried – Bezier, Cubic, and Composite. These methods did an admirable job with well-defined data, but suffered when the entire data set was noisy or there was a large spike in the data.

Moving Bezier spline interpolation is similar to moving averages, but here a Bezier spline is interpolated over the data subset and the corresponding point in the spline replaces the current data point. This method does not distort the data in regions where the 2nd derivative is quite large, and thus works better than weighted averages in those regions. However, it is still susceptible to spikes in the data.

Fourier filtering did not work very well. Using only 40 data points severely limits the upper range of frequencies that can be filtered out. Thus, any Fourier filtering of the data severely distorted the shape of the TL curve. In order for this method to work effectively, a much larger sampling of data points is necessary.

Deconvolution smoothing uses the method of deconvolution to first determine the energy components, and then these components are used to recreate a smoothed TL curve. Because the theoretical shape of a TL curve that enters into the deconvolution routine must extend over many neighbouring data points, the method does not have the freedom to fit itself to noise and spikes. A TL curve cannot simultaneously have a large value at one location and a low value at the nearest neighbour, unlike noise, where values are uncorrelated to those of neighbouring points. Thus, the routine simply ignores noise and spikes in the data ensuring that only the TL contribution is fit. If a very high frequency factor is used, the method is able to almost perfectly smooth the data. The major problem with this method is that it is the most calculation intensive of all the methods tried. On average, it was at least 30x slower using deconvolution smoothing compared to the next slowest method (moving Bezier spline interpolation). However, because of its ability to smooth the data without distortion, all smoothing of data was done using this method.

2.6 Results

Multivariate Analysis, Deconvolution and Neural Networks were applied to the training sets to determine the effectiveness of the approaches. The data was presented in both original form, normalized to unit area form, and smoothed form.

Initially, the three different methods were presented with the training data set to ensure that they were able to correctly determine the training set. The data were presented to the methods in a variety of forms. Any method that did not correctly identify all of the training data were not tested any further.

Table 2.1 lists the results determined by the three methods

In total, six different techniques were successful in correctly determining all of the training data. Table 2.2 lists the methods and the data inputs necessary to get a correct determination.

The methods that correctly determined all the training data were then used to evaluate the 10%, 1%, and 0.1% mixtures. Table 2.3 summarizes the efficiency of each method to correctly determine the mixtures along with the current methods ‘TL (1996)’ and ‘TL (1998)’.

From the data in Table 2.3, a number of methods can be eliminated because of substandard performance. Those methods are TL(1996), Neural Network-Norm G1, Neural Network-Norm G1/G2, and Neural Network-Norm D1/D2. Surprisingly, though, four of the methods performed almost identically to TL (1998) and none exceeded those values. Those methods are listed in Table 2.4.

METHOD	INPUT DATA	UNIRR %	IRR %	TOTAL CORRECT %
Multivariate Linear	G1 only	100	53.7	80.2
	Norm G1	99.1	100	99.5
	G1 / G2	100	54.9	80.7
	Norm G1 / G2	99.1	97.6	98.4
	D1 only	100	52.4	79.7
	Norm D1	100	100	100
	D1 / D2	100	56.1	81.2
	Norm D1 / D2	96.3	93.9	95.6
Multivariate Quadratic	G1 only	-	-	-
	Norm G1	99.1	100	99.5
	G1 / G2	-	-	-
	Norm G1 / G2	98.2	98.8	98.4
	D1 only	-	-	-
	Norm D1	99.1	98.8	99
	D1 / D2	95.2	97.4	96
	Norm D1 / D2	89.2	92.1	90.7
Deconvolution	Low E D1/High E D2	100	100	100
Neural Networks	Norm G1 only	100	100	100
	Norm G1 / G2	100	100	100
	Norm D1 only	100	100	100
	Norm D1 / D2	100	100	100

Table 2.1: Percentages of training data for various methods and input data sets correctly determined.

TECHNIQUE	DATA INPUT
Multivariate--Linear	Norm D1
Deconvolution	Low E D1/High E D2
Neural Network	Norm G1 only
	Norm G1 / G2
	Norm D1 only
	Norm D1 / D2

Table 2.2: Techniques that correctly determined all of the training data

METHOD	CRITERION	10%	1%	0.1%
TL (1996)	G1/G2 > 0.1	84% 91/108	35.0% 38/108	15% 15/100
TL (1998)	G1/G2 < 0.1 peak	96% 104/108	75.0% 81/108	54% 54/100
Discriminate analysis	Normalized D1	90.5% 95/105	70.0% 70/100	54.1% 53/98
Deconvolution	Low E D1/High E D2	96.1% 101/105	75.0% 75/100	54.1% 53/98
Neural Network	Norm G1	89.5% 94/105	51.0% 51/100	24.5% 24/98
	Norm G1/G2	77.1% 81/105	27.0% 27/100	13.3% 13/98
	Norm D1	94.3% 99/105	64.0% 64/100	54.1% 53/98
	Norm D1/D2	81.9% 86/105	50.0% 50/100	23.5% 23/100

Table 2.3: Performance of methods on mixtures of irradiated and unirradiated material using TL.

METHOD	CRITERION	10%	1%	0.1%
TL (1998)	G1/G2 < 0.1 peak	96% 104/108	75.0% 81/108	54% 54/100
Discriminate analysis	Normalized D1	90.5% 95/105	70.0% 70/100	54.1% 53/98
Deconvolution	Low E D1/High E D2	96.1% 101/105	75.0% 75/100	54.1% 53/98
Neural Networks	Norm D1	94.3% 99/105	64.0% 64/100	54.1% 53/98

Table 2.4: Four best methods for determining mixed grain irradiations. Notice the almost identical performance of all four methods.

The possible effects of grain statistics are considered here; currently the size distribution and grain numbers from the sample have not been determined explicitly, although the samples have been retained. The following analysis however confirms that grain statistics could indeed be one of the key considerations, which determine the success of experiments to detect low concentration blends.

Given the outcome of this analysis it may be worth investigating i.) the actual grain size distributions of the samples examined, ii.) the potential for improving performance of the 0.1% blends by taking larger samples in conjunction with the statistical approaches outlined here. It will also be necessary to address grain statistical aspects when developing procedures based on imaging and single grain approaches.

If one considers the probability of finding an irradiated grain in a mixture of unirradiated grains, the fact that four different methods determined almost identical percentages are no longer surprising. Consider, for example, the 0.1% mixtures. If one assumes that there are approximately 1000 grains on the disk, then there is a 64.23% chance of having at least one irradiated grain on the disk. This value compares very closely with the 54% that was actually determined by the four best methods. Because four different methods determined almost identical values, this would indicate that the methods are not missing 46% of the cases, but that 46% of the samples had no irradiated grains on them.

For the 0.1% mixtures, to ensure a 99% certainty that there will be at least one irradiated grain on the disk, a minimum of 4602 grains must be used. It would be expected that different mineral grains would exhibit different luminescence sensitivities, which would create an additional effect. If the irradiated grains have low sensitivity then more grains will be needed to ensure a signal is detected. The numbers actually used, though, were around 1000 grains. In order to see improvements in the performance of the four best methods, much larger numbers of grains must be used.

3. Imaging approaches

The second part of the project investigated options for instrumental development to improve detection of blended materials containing irradiated materials. The approach investigated was the use of scanning systems in which grains distributed across a disc are sequentially stimulated by a focussed laser, resulting in detected signals from small numbers of grains to be measured at one time. The result would be to produce images in which single irradiated grains would hopefully be identifiable amongst a much larger number of unirradiated grains.

3.1 IR Scanning System

A system for IR stimulation of individual mineral grains spread across a disc had been developed prior to this project. It uses a focused pulsed laser diode, with the PSL signals recorded using digital lock-in photon counting. By moving an X-Y micrometer stage, driven by stepping motors, the sample can be sequentially stimulated by the laser and hence an image formed. The system is shown schematically in figure 3.1.

When the laser stimulates a grain that has been highly irradiated, a large amount of luminescence is emitted from the grain, with corresponding low levels of luminescence from unirradiated grains. This gives rise to regions of relatively intense luminescence within regions of relatively low luminescence. Images showing regions of low luminescence emission along side regions of high luminescence emission indicate that the irradiation states of the various grains are mixed. One of the first measurements with this system, using a mixture of irradiated and unirradiated mineral grains of approximately 100µm diameter, with 100µm steps between static measurements on a pixel matrix is shown in Figure 3.2. The data capture using this method is relatively slow, however it is possible to obtain a high sensitivity image.

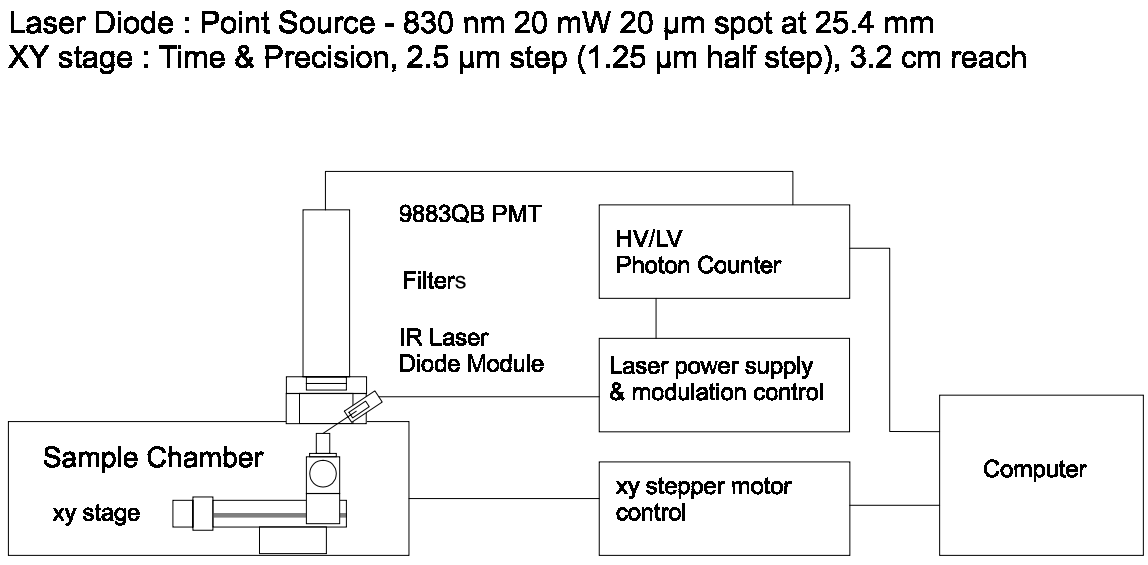

Figure 3.1: Schematic of the IR scanning system

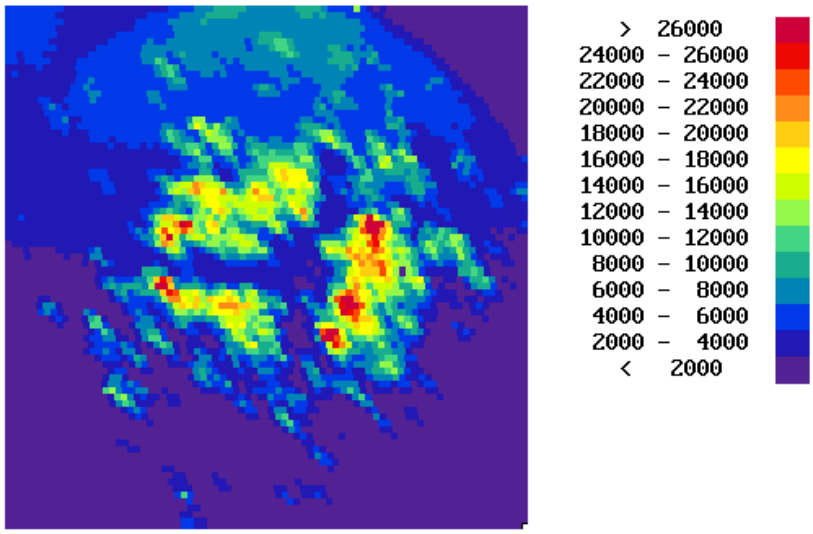

Figure 3.2: Initial IR scan of irradiated feldspar grains

3.1.1 Scanning experiments

After the initial measurements, the prototype system was modified to use a 20µm diameter 830nm 20mW laser and an XY stage capable of 2.5µm steps with a range of 15cm x 15cm. The sample holder was been raised by 8mm to obtain a more focused beam (reducing the beam spot size) and a diode fixed to the side of the sample holder to aid repositioning and alignment.

Experiments were carried out using controlled mixtures of feldspar containing 10%, 1% and 0.1% irradiated material. The feldspar blends were dispensed onto 10mm diameter stainless steel discs, sprayed with silicone grease to hold the grains in place, in the shape of a cross. During scanning the disc was moved under the laser beam in 100µm steps, comparable to the sizes of the individual grains. After each step a one second measurement was recorded. The discs were then given a 200Gy dose using a ^{90}Sr beta source, preheated at 100°C for 30 minutes and rescanned using the same setup as before. Scanning was conducted in down counting mode, where the system continually subtracts its own background. The software produces an image on the screen during measurements, allowing the operator to view the image being constructed as the data is collected. This also provides an early indication of whether there are any problems and as measurements can take several hours, early identification of unsuccessful measurements is valuable. Analysis of the data has been done through an existing program which produces 16 colour images of the disc. The scanning results are shown below in figures 3.3 and 3.4 for both 1st and 2nd scans.

The cross shaped pattern on the discs can be seen for both the 10% and 1% discs, with the 10% being significantly better pronounced, as dispensed. For the 1% disc there is no image observed, indicating that no irradiated grains had been dispensed onto the disc. Given that only a relatively small number of grains (several hundred) were dispensed this is not entirely surprising.

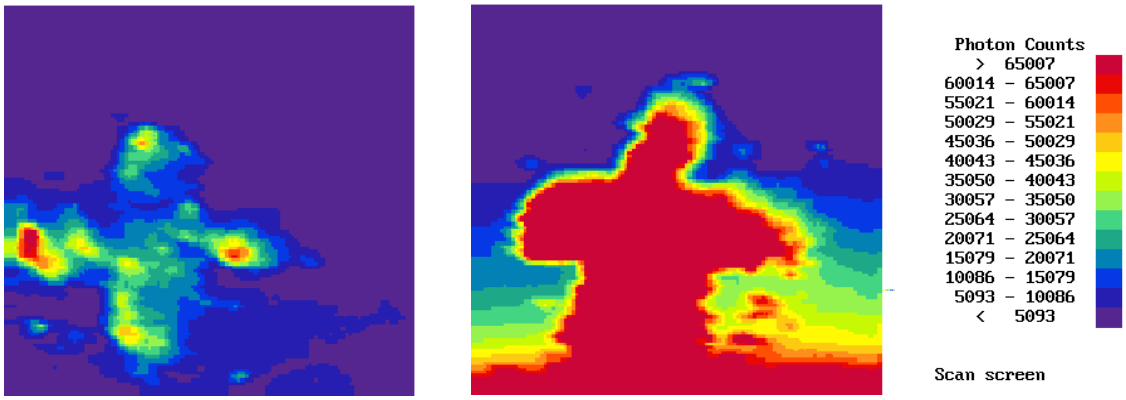

Figure 3.3: IR scans from mixed feldspar grains (90% unirradiated: 10% irradiated to a 1 kGy dose). The first scan is from the sample as dispensed; then second scan follows a 200 Gy beta dose to the whole disc.

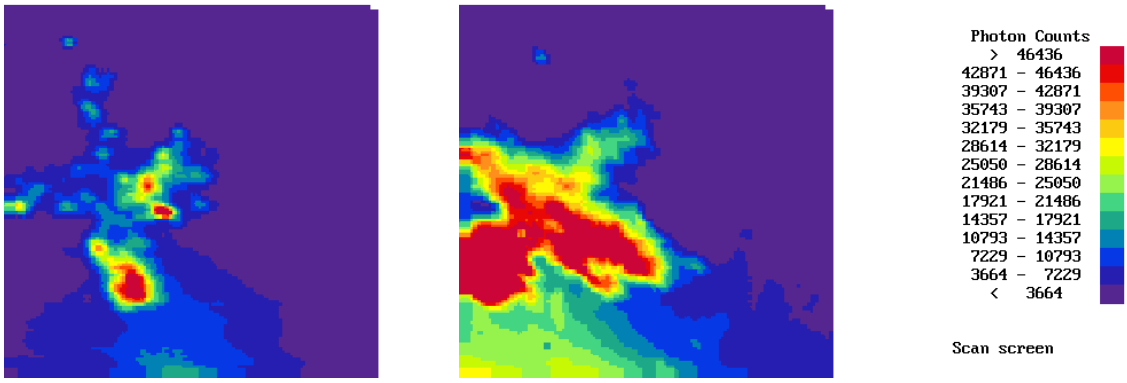

Figure 3.4: IR scans from mixed feldspar grains (99% unirradiated: 1% irradiated to a 1 kGy dose). The first scan is from the sample as dispensed; then second scan follows a 200 Gy beta dose to the whole disc.

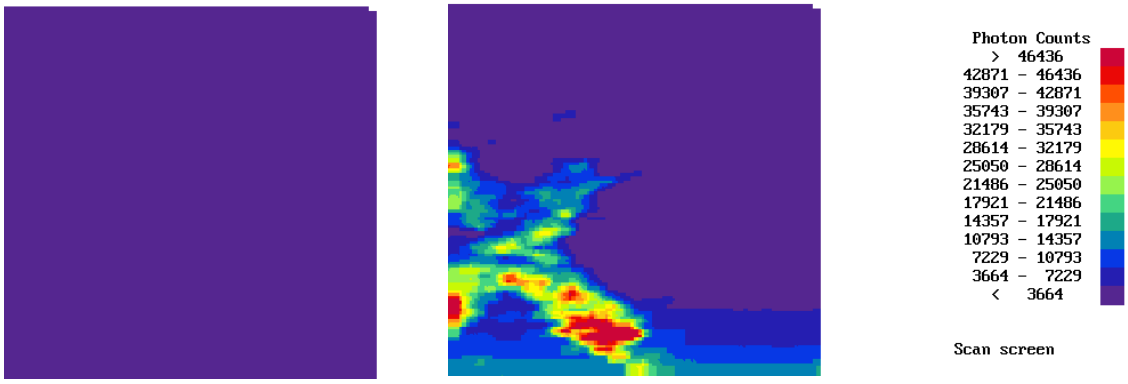

Figure 3.5: IR scans from mixed feldspar grains (99.9% unirradiated: 0.1% irradiated to a 1 kGy dose). The first scan is from the sample as dispensed; then second scan follows a 200 Gy beta dose to the whole disc.

Another problem encountered with this initial system is that of repositioning of the disc after irradiation for re-measurement. From the above scans we can see that there has been slight rotation in some cases of the disc between first and second measurements.

3.1.2 Sensitivity

The precision of the results obtained from the system and the range of applications for which it is suitable are dependant upon the minimum dose that can be detected by the system. Optimisation of the signal to background ratio of the scanning system depends on the depletion rate of signals stimulated at high power densities with a focused laser. In common with other PSL work, it is expected that the initial rate of signal depletion will decline. While it is desirable to record as many photons as possible from the luminescence emitted from each grain, unnecessary prolongation of the measurements will not only lead to decreased system throughput but also reduced signal to background ratios. For practical reasons this instrument operates with measurement times of whole numbers of seconds. This could be varied by modification of software and timing hardware, however prior to doing this, the extent of depletion in repeat scans was investigated using a 1% irradiated sample.

Two discs were sparsely covered with 1% irradiated feldspar. The sample was scanned using the usual setup and the scan was repeated for a second time. The results are shown in figure 3.6. One measurement removes most of the signal from the grains, leaving only a very small residual signal (around background levels). This indicates that for 1 second measurements the vast majority of the stored signal in each grain has been stimulated, and that the measurement is longer than is needed. Future work could involve modification of the equipment and software to allow shorter measurement times.

3.1.3 Presentation of mineral grains

Minerals have been presented to the IR system for measurement as evenly coated reflective discs. There is some evidence of laser scattering effects, which might limit the ability to detect true single grain images. This effect occurs when the laser light is not completely absorbed by the stimulated grain and scatters to other parts of the sample. This scattered light can then strike another grain on the disk, causing it to emit stimulated luminescence. This results in the amount of luminescence measured at one location on the sample being not only the luminescence emitted by the optically stimulated grain, but also the sum of the luminescence emitted from grains being excited from the scattered stimulation light. This may also deplete some of the trapped charge in the grains being excited by the scattered stimulation light, and at a later time the measured emission from these grains will then be low due to the previous depletions of the trapped charge population.

From the data collected so far, it is unclear how much of a problem this is, although it is highly unlikely that it is intense enough to deplete an irradiated grain to background levels. However, it is possible that the scattering effects limit the integrity of the images, therefore different ways of presenting the minerals on disc to the system have been investigated, with a view to the minimization of these effects.

Various methods of sample presentation have been considered to reduce this problem including:

i) Presentation of grains on adhesive, non-reflective backing materials
ii) Embedding the minerals in a thin layer of bluetack or other similarly soft material
iii) Presentation of grains in small drilled recesses in a flat disc

The results of investigation of these approaches are shown below in figures 3.7 to 3.11.

Figures 3.7 and 3.8 show scanned images for feldspar containing 1% and 0.1% irradiated material respectively. The discs are coated with a material, similar to double sided sticky tape, used for mounting samples for electron microscopy which holds the grains in place while eliminating the majority of reflections from the disc surface. The grains stand above the surface of the disc, and so there is still some cross-talk between grains.

Figure 3.9 shows scanned images for feldspar containing 1% irradiated material pressed into a thin layer of bluetack. This results in much reduced cross-talk though there is some evidence of the laser reflecting off of the material. Compared to other methods there is some additional effort required in dispensing the sample onto the disc.

For both the adhesive backing and bluetack there are potential problems with how the material would respond to preheating. Also, both of these methods would require sample preparation and dispensing to be done in ultra-clean environments as the potential for any stray minerals to adhere to the discs is very high.

Figures 3.10 and 3.11 show scanned images for feldspars containing 10% and 1% irradiated materials respectively, dispensed onto anodised discs with small drilled pits in a hexagonal pattern. The anodised surface significantly reduces reflections, while the metal surfaces in the pits allows the laser to fully illuminate the mineral grains resulting in the maximum possible luminescence signal. Each pit may hold several grains, though dispensing in a darkened environment means it is impossible to ensure all pits hold at least one grain or that there are no grains on the anodised surface. There is still some evidence of a small amount of reflection from the surface of the disc stimulating grains either on the disc surface, or which sit slightly above the surface in the pits, but the resulting background towards the top of each image is still sufficiently small that the individual pits can still be observed against it.

Figure 3.6: The effect of repeat IR scanning on signal levels obtained from a mixed feldspar sample containing 99% unirradiated grains and 1% irradiated grains.

These results indicate that:

i) Black backing seems to improve the spatial resolution of the images, in keeping with the general expectation that cutting down reflections should minimise scatter effects. However, this mode of sample presentation reduces the reflective enhancements of detection efficiency leading to lower light sums in the scans. This effect might diminish detection limits unacceptably.

ii) Pressing the grains into a soft translucent substrate, while avoiding the loss of signal sensitivity does not improve spatial resolution in comparison with flat discs. If setting samples into a resin, for example, this would need to be a light absorbing medium, which would also diminish sensitivity

iii) The drilled discs with a hexagonal matrix of 0.2mm diameter holes cut into the reflective Al behind a black anodise surface appear to combine the benefits of both approaches. Individual signals from each hole are well resolved in trials. It appears that the reflective backing is projecting the luminescence forward in the direction of the PMT resulting in high detection efficiency.

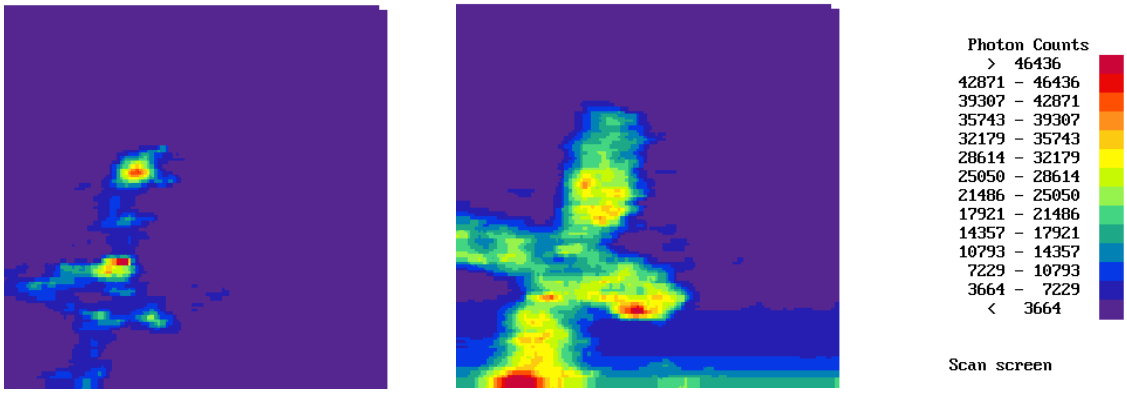

Figure 3.7: Results from mixed feldspar grains (1% irradiated) dispensed as a cross on black adhesive stubs. The first scan is from the sample as dispensed; then second scan follows a 200 Gy beta dose to the whole disc.

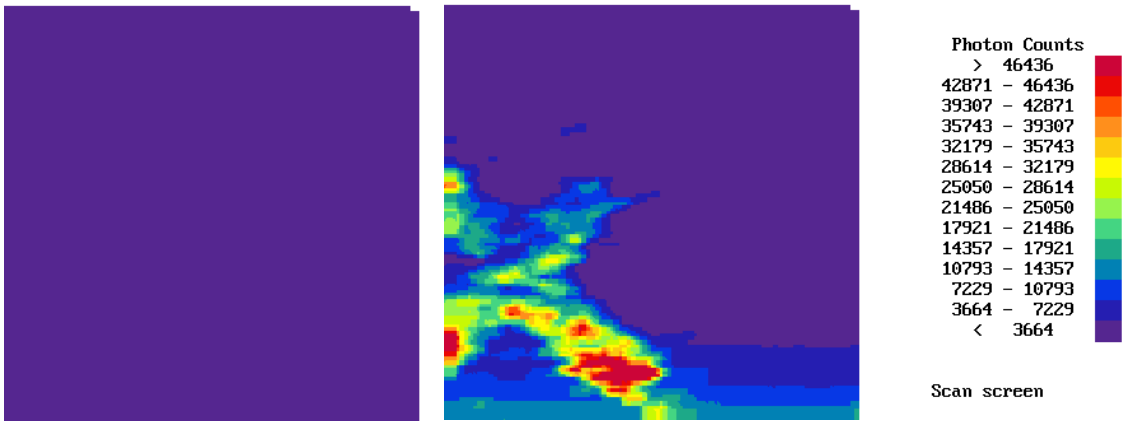

Figure 3.8: Results from mixed feldspar grains (0.1% irradiated) dispensed as a cross on black adhesive stubs. The first scan is from the sample as dispensed; then second scan follows a 200 Gy beta dose to the whole disc.

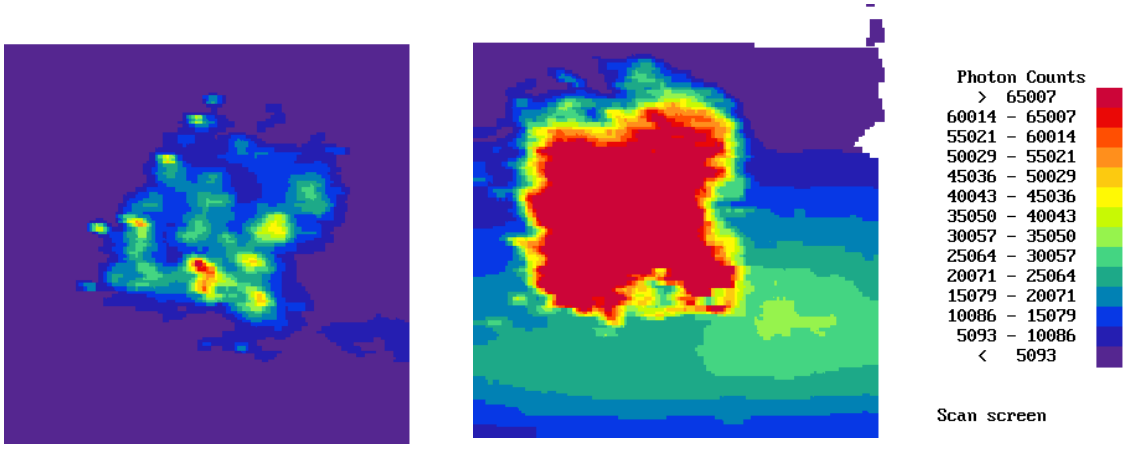

Figure 3.9: 1% Feldspar as a cross on thin layer of blue tack

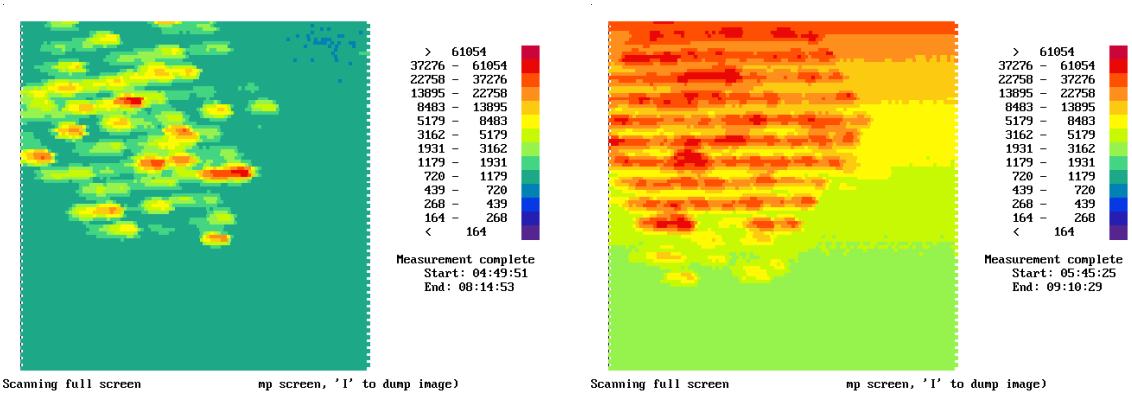

Figure 3.10: 10% Feldspar presented in a hexagonal array of drilled 0.2mm diameter holed disc

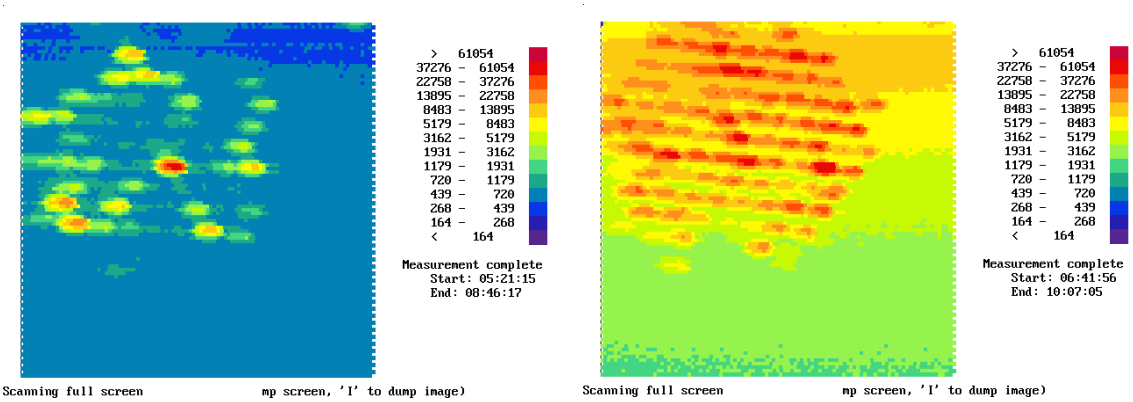

Figure 3.11: 1% Feldspar on hexagonal pitted disc

3.1.4 Quantitative Analysis of Scanned Data

By integrating the number of photon counts from each pit it is possible to do some quantitative analysis of the data from the scanning experiments. This was done by loading the data into a Geographical Information System (GIS) and using techniques developed for analysis of mapped data. A mask was produced, with each pit enclosed by a labelled circle, as shown in figure 3.12. At present the mask has to be drawn by hand, and adjusted for each scan as the disc is not located in the same place for each scan. Future developments would be needed to automate this analysis process, possibly involving developing stand alone software to perform this task. Each circle encloses 14±1 measurement locations. For the first scans, where a fairly uniform background is observed, an average background per measurement location is determined, and then subtracted from the counts for each pit taking account of the number of measurements in each circle. For the second scans, a time dependant background is observed. In these cases a larger area, enclosing approximately 30 locations, has been integrated around each pit with the difference between this and the counts for the pit itself used to define the local background. Typically, backgrounds of approximately 10^4 and 10^5 have been subtracted from the first and second scans respectively. Tables 3.1 and 3.2 give the net integrated counts for each pit for both the first and second scans, with the ratio of these, for the scan of the disc with feldspar grains containing 1% and 10% irradiated material respectively.

Previous work[12] has shown that it is possible to distinguish bulk irradiated and unirradiated material from histograms of photon counts and scatter plots of PSL signals obtained before and after irradiation, as illustrated in figure 3.13. Irradiated materials will have larger initial PSL signals, and hence in the histogram be further to the right of the plot, however there is a region where the classification from the initial signals is ambiguous. In the scatter plots, however, irradiated materials lie along the diagonal with approximately equal signals both before and after irradiation.

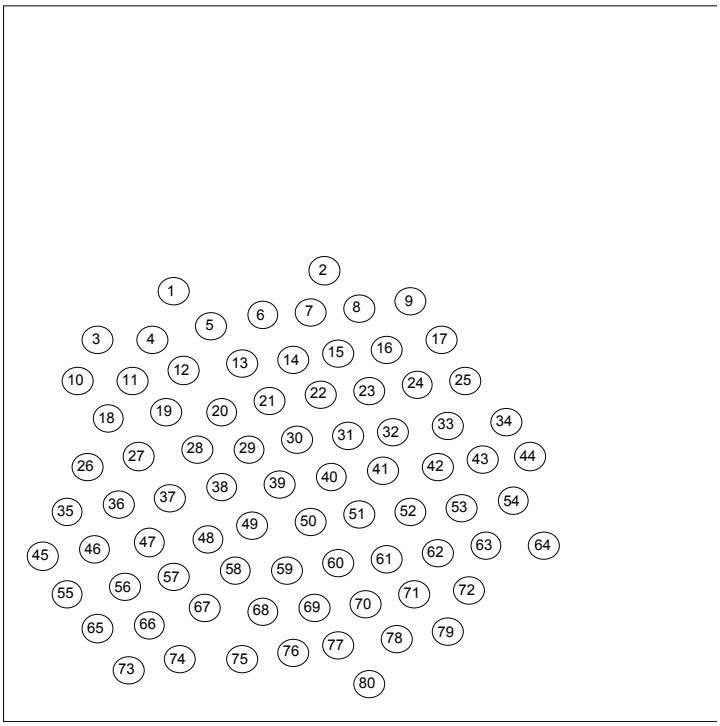

Figure 3.12: Scanned image for the 10% irradiated feldspar following re-irradiation, with the mask shown

Location	First Scan	Second Scan	Ratio	Location	First Scan	Second Scan	Ratio
1	949	51241	0.019	41	1497	122452	0.012
2	764	85398	0.009	42	27291	217020	0.126
3	187350	135169	1.386	43	658	41959	0.016
4	17779	23404	0.760	44	194	74301	0.003
5	7662	34880	0.220	45	45640	111626	0.409
6	1824	12972	0.141	46	33457	48458	0.690
7	2123	14376	0.148	47	2186	79423	0.028
8	95041	95776	0.992	48	909	74966	0.012
9	11338	83925	0.135	49	1155	152952	0.008
10	181236	118088	1.535	50	4122	126752	0.033
11	2628	62086	0.042	51	471	88351	0.005
12	66514	55652	1.195	52	1360	121553	0.011
13	2096	83643	0.025	53	12196	184769	0.066
14	1772	31854	0.056	54	54	210436	0.000
15	25637	73659	0.348	55	269	63435	0.004
16	1824	172404	0.011	56	21052	66952	0.314
17	4085	139912	0.029	57	6729	13465	0.500
18	5674	66194	0.086	58	2621	62388	0.042
19	2038	44970	0.045	59	2892	74267	0.039
20	14092	40283	0.350	60	24752	131662	0.188
21	1552	94039	0.016	61	391	127501	0.003
22	2373	78355	0.030	62	1413	110620	0.013
23	1289	44139	0.029	63	22197	178803	0.124
24	1223	26871	0.046	64	-450	89546	-0.005
25	884	80373	0.011	65	-350	60479	-0.006
26	23705	140640	0.169	66	3791	2343	1.618
27	19909	200557	0.099	67	59266	66324	0.894
28	1906	157595	0.012	68	85762	245743	0.349
29	9156	100001	0.092	69	17583	229154	0.077
30	428828	356557	1.203	70	53	169451	0.000
31	3084	124913	0.025	71	527	64545	0.008
32	11893	26604	0.447	72	1609	82537	0.019
33	79737	426647	0.187	73	-1604	111164	-0.014
34	990	120321	0.008	74	17920	66075	0.271
35	1248	94674	0.013	75	107161	239999	0.447
36	5659	101640	0.056	76	-962	134393	-0.007
37	1076	77949	0.014	77	-941	100094	-0.009
38	1235	59083	0.021	78	-846	181503	-0.005
39	5420	269759	0.020	79	-818	119956	-0.007
40	1179	68092	0.017	80	-1299	99446	-0.013

Table 3.1: Net integrated counts for each pit for first and second scans of feldspar containing 1% irradiated material

Location	First Scan	Second Scan	Ratio	Location	First Scan	Second Scan	Ratio
1	9565	141993	0.067	37	859	90446	0.010
2	60867	254425	0.239	38	2312	96136	0.024
3	4198	174950	0.024	39	2749	162810	0.017
4	32435	117883	0.275	40	165345	141138	1.172
5	53231	127575	0.417	41	7794	89338	0.087
6	130929	124746	1.050	42	91868	104861	0.876
7	4769	136190	0.035	43	13605	98413	0.138
8	60631	103438	0.586	44	33117	166254	0.199
9	21897	167798	0.130	45	8032	134885	0.060
10	13548	98871	0.137	46	81458	145973	0.558
11	894	147268	0.006	47	2749	61598	0.045
12	2094	117412	0.018	48	32080	54416	0.590
13	17651	100212	0.176	49	17907	168030	0.107
14	22149	181634	0.122	50	103781	136633	0.760
15	11620	134571	0.086	51	71906	130545	0.551
16	27683	76230	0.363	52	387584	121002	3.203
17	31330	116492	0.269	53	34382	72657	0.473
18	271519	56436	4.811	54	5419	117705	0.046
19	380977	67480	5.646	55	6031	60915	0.099
20	22003	176274	0.125	56	1131	57333	0.020
21	32413	84432	0.384	57	1574	148218	0.011
22	13130	111233	0.118	58	97889	142523	0.687
23	8752	138634	0.063	59	47979	155133	0.309
24	256171	128882	1.988	60	75996	119178	0.638
25	165208	167347	0.987	61	49265	322241	0.153
26	11830	161848	0.073	62	92168	80689	1.142
27	15074	153535	0.098	63	66719	59381	1.124
28	716	120754	0.006	64	706	156947	0.005
29	193376	157820	1.225	65	-612	90849	-0.007
30	2373	146531	0.016	66	54545	196626	0.277
31	9364	92546	0.101	67	1583	130784	0.012
32	26298	192850	0.136	68	13345	71945	0.185
33	12060	167974	0.072	69	28078	110297	0.255
34	67182	114711	0.586	70	40717	117409	0.347
35	106923	133999	0.798	71	5970	110772	0.054
36	12374	136056	0.091	72	14606	144665	0.101

Table 3.2: Net integrated counts for each pit for first and second scans of feldspar containing 10% irradiated material

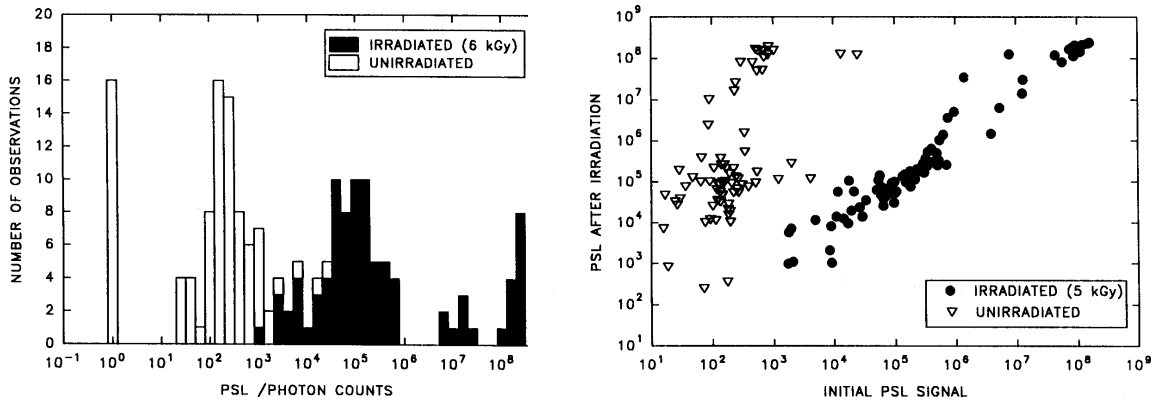

Figure 3.13: Separation of irradiated and unirradiated material using PSL, from Sanderson *et* al 1996[12]

Figure 3.14 shows plots of the second scan net photon counts against the first scan net photon counts, and histograms of the first scan net photon counts and the ratio of photon counts, for the discs containing 1% and 10% irradiated feldspar grains. The scatter plots and first scan histograms are of the same form as those shown in figure 3.13. It can be seen that the second scans show very little range in response, indicating that the sensitivity range of the material used is much narrower than that of a polymineral system such as that found from food samples. This is not entirely surprising as in this experiment the grains are all feldspar of similar sizes. There is a very much larger spread in first scan photon counts, with the 10% material showing more pits with greater photon counts. The histograms of the ratios show a substantial range, with, again, the 10% material showing more pits with higher ratios. This reflects the greater amount of irradiated material on the 10% disc. In an ideal system, there would be a clear difference between irradiated and unirradiated grains, with the irradiated grains having a large signal from the first scan, and correspondingly larger ratio to the second scan. In these experiments, there is a much more continuous distribution observed. This could be the result of factors such as the effect of multiple grains in individual pits returning signals for mixed irradiated and unirradiated grains as well as instrumental difficulties such as background subtraction issues. It is expected that further experiments with larger number of discs containing pure irradiated and unirradiated material of differing sensitivities would result in data showing similar distributions to that in figure 3.13.

Figure 3.15 shows scatter plots of the ratios of the first scan to second scan against the first scan photon counts. These clearly show that the highest ratios of photon counts correlate with the higher first scan photon counts. It is also evident with the ratios plotted on a log scale that there is a linear relationship. This indicates that the location of the mask on the two scans to identify individual pits has correctly assigned data from each pit on the first scan to the corresponding pit on the second.

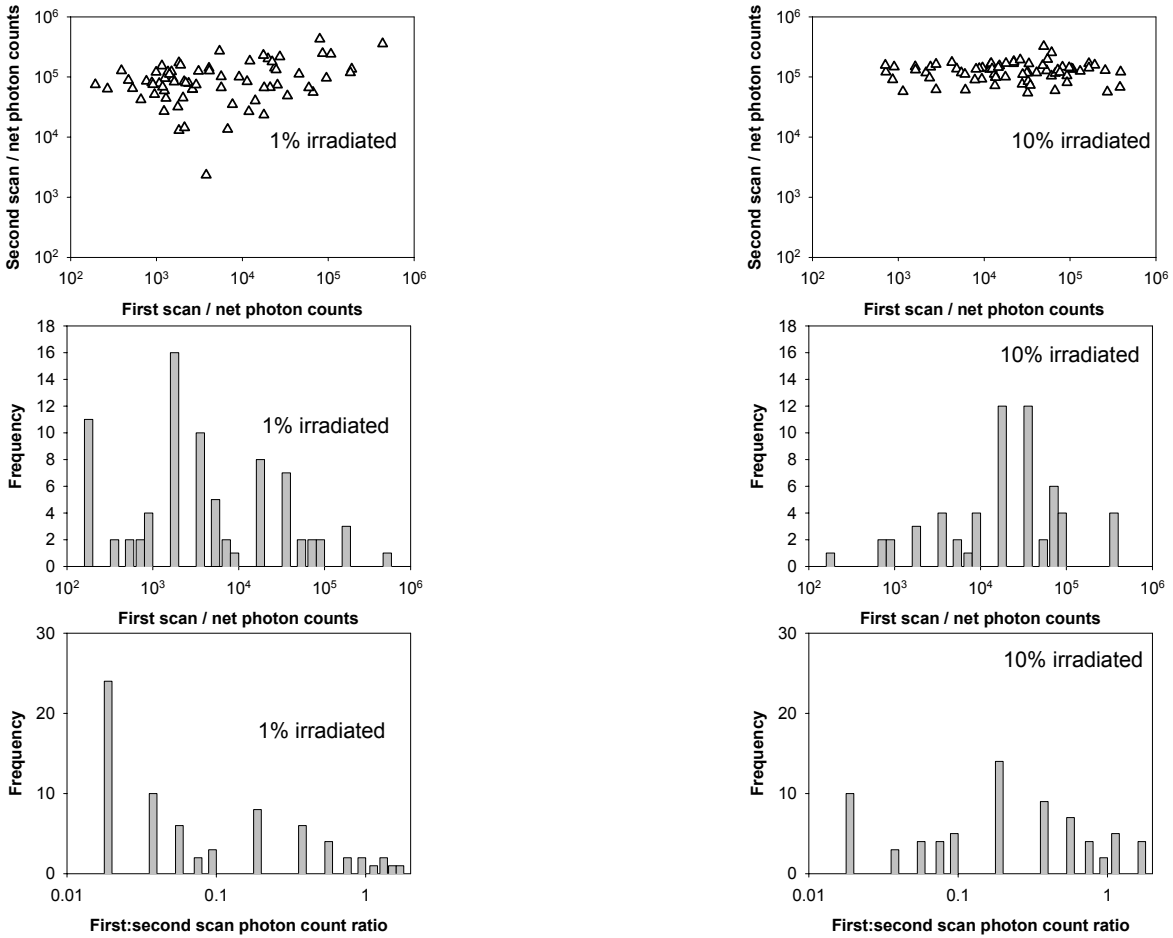

Figure 3.14: Scatter plots of second scan versus first scan, and histograms of first scan net photon counts and count ratios for discs containing 1% and 10% irradiated material

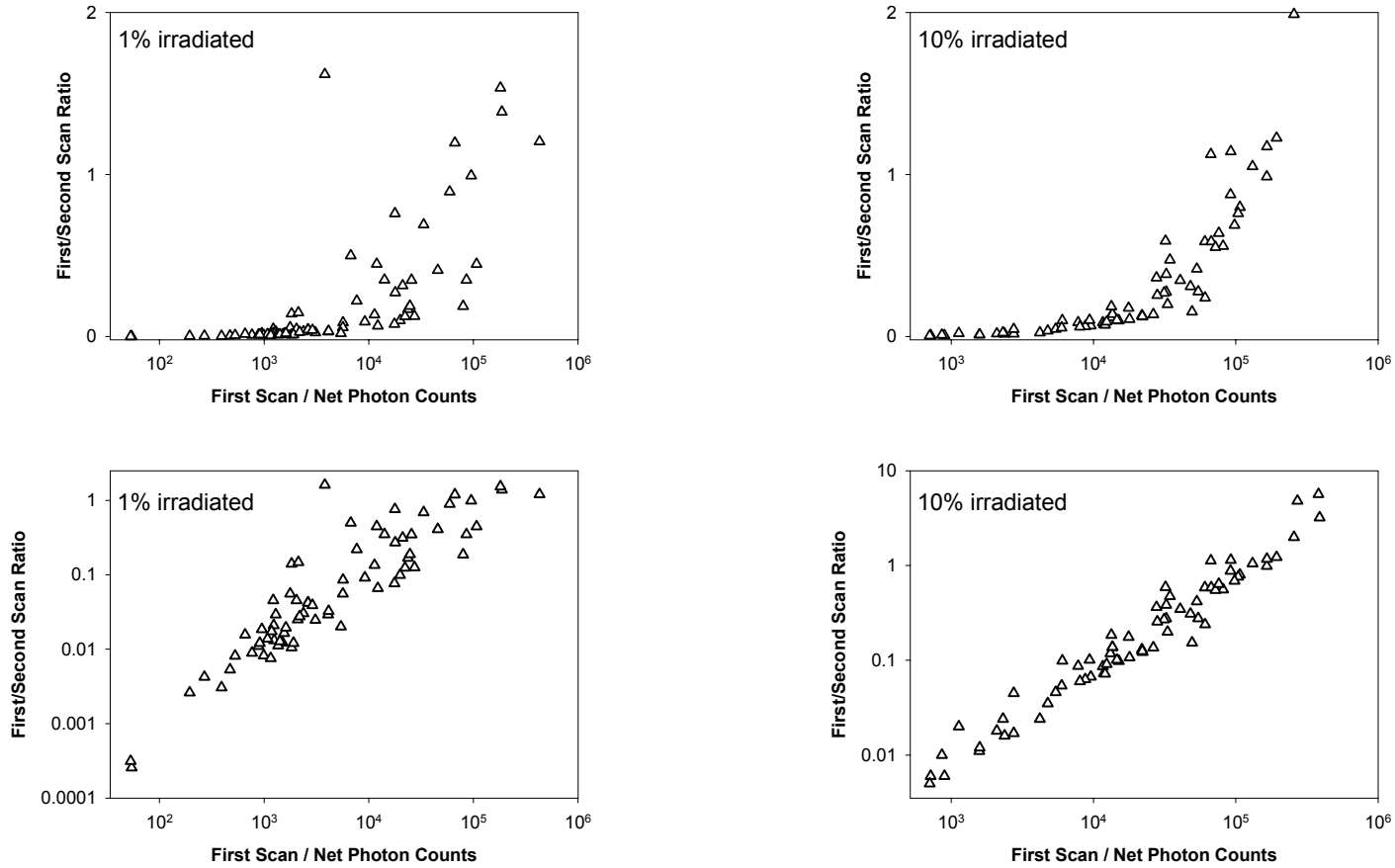

Figure 3.15: Scatter plots of the ratio of second scan to first scan, against the first scan net photon counts for discs containing 1% and 10% irradiated material.

3.2 Green Laser Imaging System

3.2.1 System Design

In parallel with the exploratory measurements using the IR scanning system; further instrumental development was underway for a secondary system capable of scanning imaging at other PSL stimulation wavelengths. Different wavelengths stimulate luminescence signals from different charge traps. In particular, shorter wavelengths (eg: from green or blue lasers) probe deeper traps in the mineral systems, and can hence be used to measure geologically induced luminescence signals either for dating purposes or to help distinguish signals in food products caused by artificial irradiation from those of natural origin.

Engineering drawing of the system were completed at SURRC and then taken to Hickinson's Engineering Company, Larkhall, to machine the components which would eventually make up the new system. This stage of the project took quite a bit longer than expected, which in turn set back the original timetable. Figure 3.16 shows a schematic diagram of the system; containing the sample chamber, collar, PM tube and laser table. A photograph of the system is shown in figure 3.17.

As with the existing system, an x-y stage is moved using two motors with 2.5μm step size- under computer control to position the disc under the focal point of the laser. A photomultiplier tube filtered with a 6mm Schott UG11 filter is used to count the photons stimulated by the laser. The laser table is positioned against the sample chamber, but has interchangeable legs and feet to allow for height adjustment to accommodate different stimulation systems. The table has positioning holes drilled to attach an "optical microbench system", as shown in figure 3.18. Microbench is used to position the laser and optics (lenses and mirror) to obtain the optimal working distance for focusing the laser and to obtain the smallest laser beam spot.

The disc is mounted on a holder on the slide within the sample chamber. The system has the choice of two holders; a single sample holder and also a 16 sample holder which are easily interchangeable. The sample holders are designed to hold the pitted anodised discs in the centre of the scanning area, in precisely fixed positions. The entire holder is removed for irradiation prior to the second scan. The overall result is that the images for sequential scans align almost perfectly so little additional effort is needed to account for differences in the positions of the pits between scans during quantitative analysis.

Scanning is conducted using continuous laser operation, stepping across the entire disc and pausing after each step to record counts. Initially measurement were carried out using the green laser LCM-LL-01CCS250 frequency doubled Nd:YAG laser operating at 532nm with a power of 0.3mW. However, after only 12 working hours the laser failed. This was replaced with a similar green laser operating at 532nm with a power of 1mW and a beam diameter of less than 0.5mm.

Two custom made collars; a single port hole and the other with 6 LED ports, were designed for this system to accommodate filters and LED's, required for alternative modes of stimulation. Presently the single port holed collar with a 12mm diameter 530 interference filter is used.

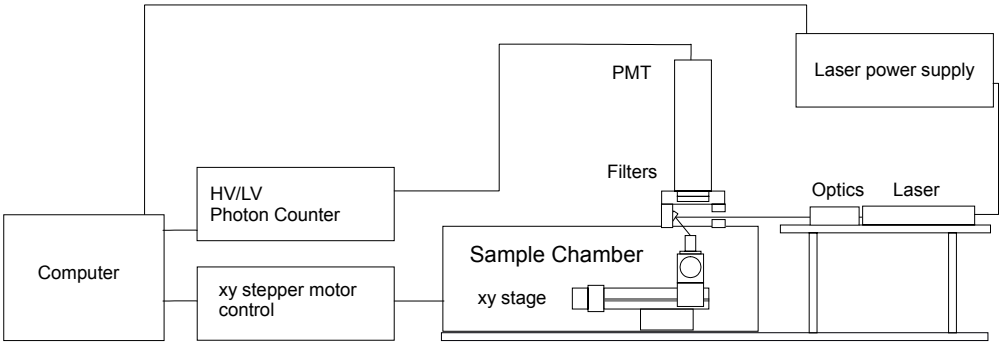

Figure 3.16: Schematic of second scanning system

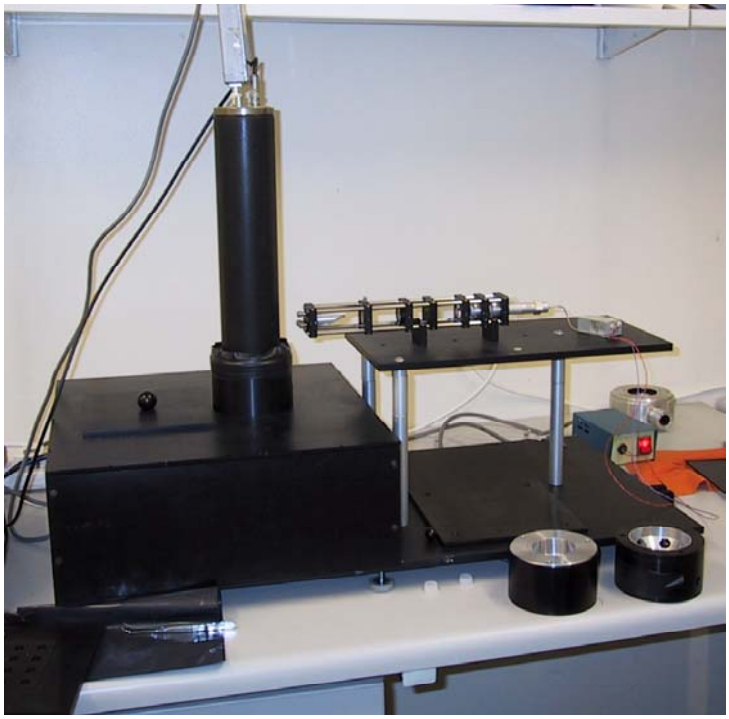

Figure 3.17: The second scanning system

Figure 3.18: Microbench setup

3.2.2 Scanning Experiments

Initial measurements were conducted to optimise the signal to background ratio, and also produce detectable signals from a highly irradiated standard material to evaluate the system performance.

Figure 3.19 shows scans of feldspar grains (0.1% of which were irradiated) distributed into the pits of the anodised Al discs, with a second scan following irradiation of the entire disc with a 200 Gy dose, using the green laser system. Although the higher energy photons of green lasers result in luminescence from deeper traps than the IR laser, and hence it would be expected to generate stronger signals, the signals recorded on these images are smaller than those observed with the IR system due to the significantly reduced power of the laser used (1mW compared to 20mW for the IR system). Even with the 200 Gy dose, the signals are not very intense.

It can be seen that even with just 0.1% of the grains irradiated, and hence it is quite likely that none of the grains on this disc have been irradiated, each of the pits generates a signal with this system. This is most likely due to a combination of luminescence signals due to geological doses excited by the higher energy of the green laser compared to the IR system and some laser light reflected from the pits passing through the filter to the photomultiplier.

It can also be seen that the discs are much better positioned with this system compared to the first IR system. They are located centrally within the scanning area, and all the scans show that the pits are in almost exactly the same position. This makes quantitative analysis similar to that conducted for the scans with the IR system much simpler, though there was very little data collected with this system so such analysis has not been done.

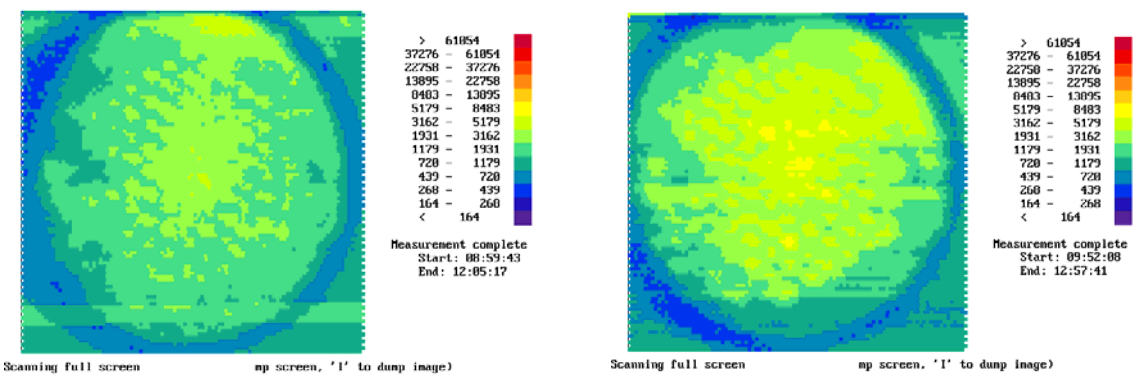

Figure 3.19: Scans of a pitted disc containing feldspar grains (with 0.1% of grains irradiated), using the green laser system.

3.3 Proposed Scanning TL System

A modification to the system outlined above will enable it to heat single grains. This will enable the system to perform both PSL measurements and TL measurements as illustrated in Figure 3.20. However, because the grain sizes are relatively small, the amount of luminescence emitted during a TL measurement will be relatively weak.

The amount of luminescence emitted from a material during a TL measurement is proportional to the total number of trapped charge carriers and the total number of recombination centres. As one shrinks the size of the sample, the amount of TL emission over the course of an experiment generally decreases. Using conventional TL heating rates ($\beta \leq 10$ Ks^{-1}), the TL emission from single grain samples whose size is on the order of 100 μm approaches the minimum detection limit of the equipment. Fortunately, the total integrated luminescence emitted from an irradiated sample during a TL measurement is constant and independent of heating rate.[†] If at one heating rate the collected emission is too weak, the heating rate can be increased, thereby, releasing more luminescence per unit time and increasing the amount of light delivered to the photomultiplier tube. This means that samples that are marginally measurable at a 'low' heating rate can be easily measured at higher heating rates.

Unfortunately, the current heating rate used in the TL instruments is 5 Ks^{-1}. This is nearing the upper limit for heating rates using a conventional electrical heating system. The main reason for this limit is that the thermal mass of the system (heater, material, planchet, sample, wires, etc.) is such that it is impossible to obtain a linear heating rate over the entire temperature range. An additional problem is that if heating rates exceed ~ 10 Ks^{-1}, the thermal gradient between the sample temperature and the thermocouple temperature increases to an unacceptably large amount.

To overcome these problems, a CO_2 laser with emission at 10.6 μm will be used to directly stimulate the samples. At these wavelengths, the energy of the light will be directly absorbed by the sample and cause the sample to heat up when stimulated by the laser. A number of groups have obtained heating rates of up to 10^4 Ks^{-1} with CO_2 stimulation indicating that it is a feasible method[13-17]. The main advantage to using a laser based heating system is that a much quicker and finer control of the heating rate is possible because we are *directly* heating the material instead of *indirectly* heating it by heating a bulky, and massive heater. In short, when the laser light is decreased, the sample temperature instantly responds, whereas when the power of a heater is reduced, the thermal momentum associated with the mass takes the heater, and thus the sample, a finite time to respond.

One potential problem with this approach is if the materials suffer from thermal quenching of the luminescence centres. In many luminescent materials, a non-radiative recombination pathway exists and competes with the radiative recombination pathway. The capture cross-sections of these two pathways are temperature dependent. At a low heating rate, the radiative pathway is dominant and a large TL luminescence signal is measured. Higher heating rates result in the TL peak shifting to higher temperatures and, at some point, the non-radiative pathway can become dominant. This leads to an overall decrease in the total integrated TL emission.

[†] The effects of thermal quenching are not considered here. If the material does exhibit thermal quenching, then the total integrated TL emission is dependant on the heating rate.

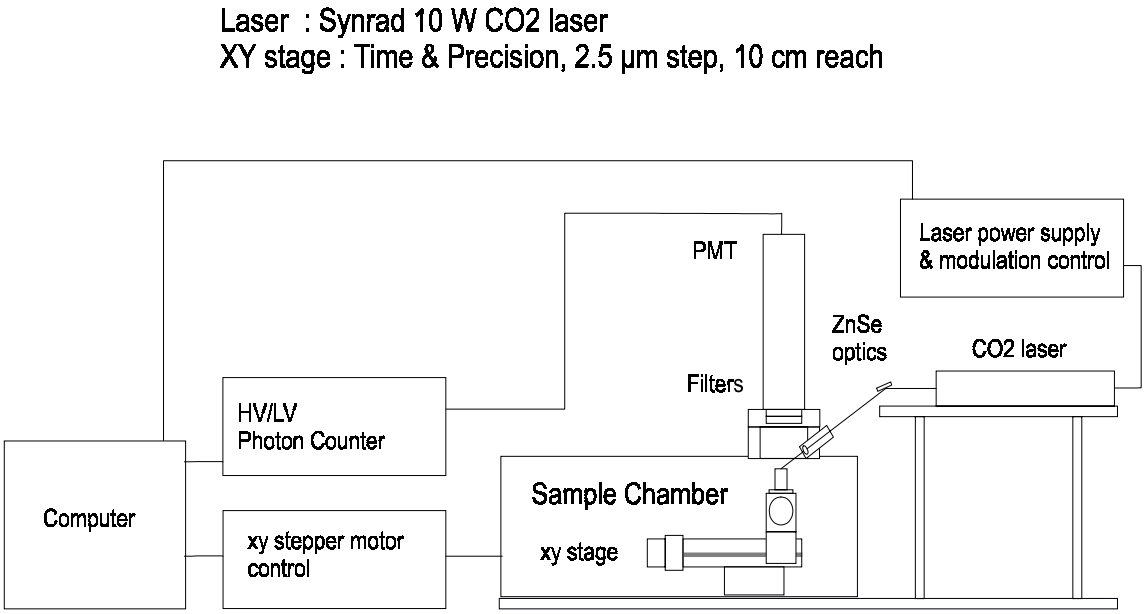

Figure 3.20: Schematic diagram of the heating system

To date, the CO_2 system has not been implemented practically, although the second scanning instrument, PMT collar arrangement and laser table have been put together in a manner which would permit practical investigation of this scheme in future work. Arguably the heating scheme will provide additional discrimination compared with the IR stimulation single grain or small aliquot approach using many drilled discs to present sample grains. On the other hand the signal to background ratios available from simple PSL scanning with drilled discs may well be sufficient to improve the performance of conventional PSL measurements to deal with blended mixtures. In which case the need for single grain TL could sensibly be reviewed when the performance limits of single grain PSL have been explored further.

4. Discussion

To summarise, the project aimed to explore a combination of statistical and imaging approaches to improving detection systems for irradiated ingredients in blended foods. This report has outlined progress and results for statistical techniques that can be used to improve objectivity and potentially performance for classifying TL data. Exploratory work has also been conducted to examine scanning imaging approaches to analysis of mineral extracts at or close to single grain levels.

Data sets from TL samples believed to be unirradiated or irradiated were identified and integrated into 10°C intervals for use in exploring statistical methods. A performance evaluation data set was also used based on the analyses of controlled mixtures of herbs and spices containing 0.1%, 1% and 10% irradiated materials. Multivariate approaches were investigated taking each TL glow curves as a 32 or 40 variable vector. Linear discriminant analyses require essentially uncorrelated data and therefore principal component analysis was applied to reduce dimensionality. The first 3 principal components contained approximately 94% of the variation in the data, 7 components accounting for 99% of the variation. These 7 component scores were used for linear and quadratic discriminant analyses. The second approach examined used kinetic deconvolution of the luminescence glow curves based on equations describing first order luminescence kinetics from a distribution of a thermal trap depth. A non-negative least squares algorithm was used to transform measured glow curves into energy spectra indicating the distance of trap charge as a function of trap depth. This approach proved highly successful in enhancing the resolution between relatively unstable signals from recent irradiation and residual signals from deep traps retaining geological signals. The third approach involved an evaluation of neural approaches of data analysis for classification. A number of neural approaches were considered briefly and one of these, the back propagation network (BPN) was investigated using custom software prepared for the purpose.

It was realised that these three main techniques could be used effectively in combination and therefore it was decided to explore such combinations as well as the main approaches originally envisaged in the proposal. The approaches that correctly determined all the training data were multivariate approaches coupled to deconvolution, a simple classification of deconvolved data, and neural network approaches based either on normalised glow shapes or deconvolved data. The conventional analysis of glow ratios also achieves the same performance for the training set. The four best methods for detecting mixed grain status were the 1998 EN standard specification which combines glow ratio analysis with visual classification of G1 peak shape, discriminant analysis applied to deconvolved glow shapes, simple classification of deconvolved glow curve data, and neural analysis of the deconvolved first glow data. Of these it might be argued that neural analysis coupled to deconvolution increase the objectivity of classification without compromising performance. It was also realised that some of the dilute blends may have remained undetected as a consequence of their limited grain statistics.

This stage of the project has, therefore, been successful in developing and demonstrating a powerful set of new approaches to dealing with TL data from dilute mixtures. It has also raised questions of grain statistics which may lead to further improvements if coupled to revised sample preparation schemes.

Exploratory work has also been conducted using scanning approaches. A system, which will record PSL using IR stimulation, had previously been assembled. Exploratory experiments have shown that images for unirradiated, irradiated and blended F1 feldspar can be obtained.

One problem encountered has been the grain-grain cross talk; a problem which arises when the laser light is not completely absorbed by the stimulated grain but scatters to stimulate other grains on the disc. Further work to minimise and improve the system has been implemented successfully based on an array of pre-drilled holes in sample discs. Methods for quantitative analysis of the scanned data have been developed, and examples of these analyses indicate that they have the potential to identify small quantities of irradiated material within a blend. Some further work to optimise these analyses is needed. In particular, the positioning of the disc allowed translation and rotation of the sample following irradiation requiring each pit to be relocated manually with each scan. Also, the measurement from each pit included a background that varied across the disc, particularly following irradiation. A method of determining the local background has been used, though it would be preferable if instrumental and procedural improvements were to significantly reduce this background prior to analysis.

A second scanning instrument has been assembled which provides practical solutions to both the scattering problems and the problem of re-positioning samples between first and subsequent scans. Provision has also been made for measuring trays of 16 samples, which can be automatically irradiated using existing beta sources, and for configuration of the laser system to explore other stimulation schemes. The system has shown that it is capable of detecting single grains. However, there is further potential to improve the resolution of the system. Initial experiments have shown that with a smaller laser beam spot size the system can be improved.

As the IR system generates larger signals, and is less influenced by geological systems, it is probably best suited to analysis of grains derived from food materials for the detection of low concentrations of irradiated components. At present, the new instrument has not been used with this laser, although fitting it would be a relatively simple procedure. A considerable number of experimental measurements with known samples will be needed to fully characterise the response of the system to irradiated and unirradiated minerals. These should include both fully irradiated and unirradiated samples, and samples of different minerals and grain sizes to provide a much greater range in sensitivity. Considerations must also be given to grain statistics, especially when measuring small sub samples of products containing an irradiated component. The multi-sample carrier should in principle be able to extend single tray statistics to >1000 subsample compartments. From a grain statistical perspective this should provide sufficient sample even in single grain form to provide a reliable basis for detection down to 0.1-1% concentrations. If small numbers of grains per hole can be accepted, and earlier work on bulk sample mixing has shown that 10% dilutions are reliably detected using conventional means, then preparations with 5-10 grains per hole may be viable and provide a means of detection at or below 0.1% concentrations.

A modification of the PSL system is in the works that will allow TL analysis to be performed on single grains. Instead of using conventional electrical heaters, a 10 W CO_2 laser with emission at 10.6 μm is directed onto the sample. At these wavelengths, the energy of the laser is absorbed by the sample and converted to heat. This allows a much quicker and finer control of the heating rate compared to an electrical heater. Higher heating rates are necessary in order to increase the TL intensity from single grains to a measurable level. Not only will the use of a CO_2 laser increase the heating rates by several orders, it will also increase the measurement throughput by decreasing the amount of time necessary to perform a TL measurement. One potential problem associated with these high heating rates is the possibility of thermal quenching of the TL emission centres. It is currently unknown if thermal quenching does exist in these materials and if so how much of an effect it will have on the measured TL.

This will need to be investigated in the future. Meanwhile it can be concluded that the work undertaken to date provides a proof of concept for the imaging/single grain approaches to luminescence detection. The systems developed in the course of this work can now be evaluated in future work with a view to improving conventional detection methods.

5. Conclusions

This study has investigated methods of improving the detection of small quantities of irradiated material within blended samples.

An investigation of statistical approaches to the analysis of TL measurements of samples containing small proportions of irradiated material has shown that several methods can identify the presence of irradiated material equally well. None of these are significantly better than analysis by a human expert.

The controlling factor for detection of low levels of irradiated component within a sample is the number of grains in the sample. For a sample containing 0.1% of irradiated material, over 4000 grains would be needed to give a 99% chance of having one irradiated grain in the sample. The standard TL method typically uses about 1000 grains for such analysis. An increase in the sample size would improve detection of small quantities of irradiated material in a blended sample.

One approach to increasing the sample size would be to employ the techniques used for mineral extraction prior to TL analysis to samples used for PSL, thus increasing the number of grains in a PSL measurement. As it is expected that different ingredients in a blend would have different minerals associated with them, another potential approach would be to extract different mineral fractions and measure TL on each separately. This would increase the proportion of irradiated grains in the fractions associated with the irradiated material.

An instrumental approach, in which the grains are distributed across a disc which is then scanned by a laser for PSL analysis, has also been investigated. This would, potentially, allow the luminescence from single irradiated grains to be measured with improvements to the signal to background ratio. Preliminary experiments have identified some potential problems in this approach, most significantly through cross-talk between grains. The use of anodised discs, with a number of small drilled pits to hold the grains, has successfully reduced this effect by a significant amount.

The prototype instrument has been tested using IR and green laser systems. The use of two wavelengths stimulates different traps within the minerals, resulting in different sensitivities to geological and artificially induced irradiation. There is some potential, which has yet to be explored, in the use of two lasers for PSL to improve signal to background ratios.

A method for quantitative analysis of the data collected by such imaging systems has been demonstrated. Some additional work is needed to account for backgrounds in the measurements and fully characterise the system.

There is also the possibility of using laser-heating to conduct TL measurements using this scanning system. Again, there has been insufficient time within this study to investigate this option.

The prototype system also has the capability to use a multi-disc holder. This would enable the measurement of several samples automatically, thus increasing sample through-put and the size of samples that can be scanned. As noted earlier, the number of grains measured is the controlling factor in identifying the presence of low quantities of irradiated material in blended samples.

References

1. Statutory Instruments 1990, The Food Labelling (Amendment) (Irradiated Food) Regulations, 1990, SI 1990:2489

2. Statutory Instruments 1996, The Food Labelling Regulations 1996, SI 1996:1499, HMSO

3. EN, 1997, Foodstuffs – Detection of irradiated food from which silicate minerals can be isolated: Method by Thermoluminescence, BS EN 1788, BSI, London

4. EN, 2002, Detection of irradiated food using photostimulated luminescence, BS EN 13751, BSI, London

5. A preliminary investigation of the impact of blending on luminescence detection of irradiated herbs and spices, 1999, MAFF Project CSA4790

6. Randall, J.T. and Wilkins, M.H.F. Phosphorescence and Electron Traps. I. The study of trap distributions. Proc. R. Soc. A **184,** 366-389 (1945)

7. McKeever, S.W.S. and Horoeitz, Y.S. Charge Trapping Mechanisms and Microdosimetric Processes in Lithium Fluoride. Radiat. Phys. Chem. **36**, 35-46 (1990)

8. Press, W.H., Teukolsky, S.A., Vetterling, W.T., Flannery, B.P. Numerical Recipies in C : The Art of Scientific Computing, Cambridge University Press (1993)

9. Lawson, C.L. and Hanson, R.J. Solving Least Squares Problems, Prentice-Hall (1994)

10. Agersnap Larsen, A., Whitley, V.H. and McKeever, S.W.S., Determination of Trap Distribution using Thermally Stimulated Conductivity. In press

11. Bishop, C.M. Neural Networks for Pattern Recognition, Clarendon Press (1995)

12. Sanderson, D.C.W., Carmichael, L.A., Naylor, J.D. Recent Advances in Thermoluminescence and Photostimulated Luminescence Detection Methods for Irradiated *Foods. Detection Methods for Irradiated Foods* (1996), 124-138.

13. Abtahi, A., Braunlich, P., Kelly, P., Gasiot, J. Laser stimulated thermoluminescence, J.Appl.Phys. **58** (4), 1985

14. Braunlich, P., Gasiot, J., Fillard, J.P., and Castagne, M. Laser heating of thermoluminescent dielectric layers, Appl.Phys.Lett**. 39** (9) 1981

15. Grupen, M., and Kearfott, K. Numerical analysis of infrared laser heating in thermoluminescent material layers, J.Appl.Phys**. 64** (3), 1988

16. Grupen-Shemansky, M.E., Kearfott, K.J., Hirleman, E.D., Numerical analysis of infrared laser heating in thermoluminescent layers: The focus laser case, J.Appl.Phys**. 66** (7), 1989

17. Gasiot, J., Braunlich, P., Fillard, J.P., Laser heating in thermoluminescence dosimetry, J.Appl.Phys**. 53** (7), 1982